Stony Brook University

The Significance of Irvine- A Possible Martian Analogue of a Terrestrial Tholeiite and its Petrologic Implications for Crustal Diversity on Mars

A Thesis Presented

by

Andrea Dawn Harrington

to

The Graduate School

in Partial fulfillment of the

Requirements

for the Degree of

Master of Science

in

Geosciences

Stony Brook University

May 2009

Stony Brook University

The Graduate School

Andrea Dawn Harrington

We, the thesis committee for the above candidate for the
Master of Science degree, hereby recommend
acceptance of this thesis.

Dr. Hanna Nekvasil – Thesis Advisor
Professor, Department of Geosciences

Dr. Scott M. McLennan – Chairperson of Defense
Professor, Department of Geosciences

Dr. Timothy D. Glotch
Assistant Professor, Department of Geosciences

This thesis is accepted by the Graduate School

Lawrence Martin
Dean of the Graduate School

Abstract of the Thesis

The Significance of Irvine- A Possible Martian Analogue of a Terrestrial Tholeiite and its Petrologic Implications for Crustal Diversity on Mars

by

Andrea Dawn Harrington

Master of Science

in

Geosciences

Stony Brook University

2009

Irvine is a fine-grained subalkalic rock found on the summit of Husband Hill within Gusev Crater, Mars. Phase equilibrium experiments were performed on a synthetic mixture of Irvine composition to better understand the nature of the igneous compositional diversity that could arise upon fractionation of a magma with this composition accompanied by the ascent of residual liquids to the surface. Since both pressure and water content are known to affect crystallization and therefore the liquid evolution, both of these variables were examined in two different studies. The former study was done under both high (9.3 kbars) and low (2.8 kbars) pressure. Although the experiments under high pressure conditions were a success, the graphite capsules used buffered the oxygen fugacity of the lower pressure experiments at unacceptably low values, causing the stability of Fe-metal in these experiments. Three water contents were

also investigated: “dry” (0.01 wt.% water), “moderately wet” (1.0 wt.% water), and “wet” (2.0 wt.% water). The experiments run under “dry” and “moderately wet” conditions yielded residual liquids that eventually showed a silica depletion trend with decreasing temperature. The “dry” and “moderately wet” trends of liquid evolution were nearly identical for all the major oxide constituents with the exception of FeO which increased along the “dry” path and decreased along the “moderately wet” path. This Fe-depletion trend observed along the “moderately wet” path, coupled with the P- and Ti-enrichment, leads to liquids that approach the Wishstone class rock compositions (rocks that were also found on Husband Hill). The silica depletion trend seen under “moderately wet” conditions appears driven by the low calcium content of Irvine, which inhibits amphibole crystallization before plagioclase is stable. The lack of amphibole and the crystallization of abundant pigeonite, and eventually plagioclase, inhibit silica enrichment of residual liquids. Thus, basaltic liquids remain basaltic during fractionation at depth and contribute to forming a basaltic martian exterior once they ascend to the surface. Although the retention of basaltic character after extensive fractionation characterizes the behavior of terrestrial tholeiite at similar pressures, the change to silica-enriched liquids is observed for water contents that exceed 0.5 wt.%. In contrast, the Irvine bulk composition still produced silica-depletion trends at 1.0 wt.% bulk water.

Table of Contents

List of Tables

List of Figures

Acknowledgements

I would like to thank…

… my advisor, Hanna Nekvasil, not only for her help with my thesis and accompanying research but also for giving me greater insight into the scientific process.

… the Geosciences Staff, especially Loretta Budd and Owen Evans, for their proficiency in being go-to people and for their knack in knowing, at least, where to go for answers.

… Don Lindsley, petrology extraordinaire, whose guidance in the laboratory was a big part of my success.

… my committee, Scott McLennan and Tim Glotch, your time and input was greatly appreciated.

… the WISE program, in particular Sharon Pavulaan, Doreen Aveni and Carrie-Ann Miller, for not only a year of funding but also for being constant cheerleaders.

… my friends, in particular Francis and Emily, for their open ears and constant encouragement that allowed me to get through the hard times.

… Alex, my best friend and fiancé, without your patience and understanding the completion of this work might not have been possible.

And finally, I would like to thank my family, especially my parents, without their support and love I might not have had the drive needed to even begin.

Introduction

Overview and Organization of Thesis

1. OVERVIEW OF THESIS

The martian crust can be subdivided into a primary and secondary crust. The primary crust represents the crust that formed during early planet-wide magma-ocean differentiation; the secondary crust represents all material that was added to the crust during the post-magma ocean period (Taylor, 2001; Wieczorek and Zuber, 2004). The Mars Exploration Rover (MER) missions and orbital remote sensing data have been used to provide new insights into the compositional nature of the top layer of the secondary crust. While it is likely that the martian surface has a wide range of rock types, based on orbital and rover analyses, the martian surface appears dominated by basaltic material. However, this does not preclude the presence of silica-rich lithologies within the martian crust, considering that only a small area of the surface has been explored in detail and that the footprint of orbital analyses is quite large (Mars Global Surveyor (MGS) has a Thermal Emission Spectrometer (TES) with a 3 km/pix footprint and Mars Odyssey (MO) has a Thermal Emission Imaging System (THEMIS) with a 100 km/pix footprint). In fact, orbital infrared data have identified localized regions of high silica on the martian surface (Bandfield et al., 2004; Christensen et al., 2005). A variety of sedimentary processes and products, as well as alteration assemblages, further add to the compositional diversity of the surface (Hurowitz et al., 2006; Ming et al., 2006; Bishop et al., 2009)

This work focuses on assessing the compositional characteristics of the magmas added to the surface and near-surface environment during the formation of the secondary crust. Since such rocks likely formed the substrate upon which many of the alteration processes acted, knowing the nature of the substrate is an important part of constraining the alteration processes and the compositional nature of the water and/or acid volatiles associated with the formation of such assemblages (Ming et al., 2006). Furthermore, such information is vital for interpreting remote spectra from MGS, MO, and Mars Reconnaissance Orbiter (MRO) (using TES, THEMIS, Compact Reconnaissance Imaging Spectrometer for Mars (CRISM), respectively), as well as MEX-Omega. Identification of lithology types on both a small and regional scale will in turn provide information on the nature of the igneous processes that may have modified primary mantle-derived melts.

This work is specifically aimed at predicting surface compositional diversity that could arise from the process of fractional crystallization of martian mantle-derived magmas, at or near the base of the crust. Given the thickness of the martian crust (Wieczorek and Zuber, 2004; Taylor, et al., 2006), the likely presence of a density barrier to the ascent of mantle-derived magmas (represented by the primary crust), and the wide-scale evidence for deep-seated fractionation processes in intra-plate regions with thick crust on Earth, assessment of the nature of evolved magmas from such fractionation is an important part of understanding martian igneous diversity. Crystallization experiments were performed on a martian lithology in order to simulate this geologic process on Mars. The Gusev Crater rock Irvine was chosen for this work because it fit numerous criteria that will be explored in depth within Chapter 1.

2. ORGANIZATION OF THESIS

This M.S. thesis is comprised of three sections, an introduction and two chapters, which are focused on the development of igneous crustal diversity on Mars. The introduction establishes the specific focus of the experiments conducted, the nature of the questions that they were designed to answer, the selection of starting compositions, and the reasons behind the choice of the pressures and water contents used in the experiments.

Chapter 1, the core of this thesis, explores the effect of water on the nature of the mineral assemblages and residual melts produced during crystallization of a martian magma, with the composition of Irvine, at the base of a thick crust. The three water contents studied were: "dry" (0.01 wt.% water), "moderately wet" (1.0 wt.% water) and "wet" (2.0 wt.% water). The water contents chosen represent those used in previous studies that brought about significant trend variations and are thought to be reasonable for low degrees (5-15%) of partial melting of the martian mantle (McCubbin et al., 2008). This chapter also offers a comparison to the assemblages produced by equilibrium crystallization experiments performed on the Gusev Crater picrobasalt Humphrey.

Chapter 2 addresses the effect that pressure has on the phase relations of crystallization experiments performed on Irvine. The experiments in Chapter 1 performed under "dry" conditions were used as the data for the high pressure study (9.3 kbars) simulating the base of Mars' thick crust and further crystallization experiments were performed at lower pressure (2.8 kbars) simulating martian mid-crustal regions. However, due to an experimental design flaw, the system at low pressure is very

reducing. Thus an additional variable, oxygen fugacity, was introduced, making comparison with the higher pressure data complicated.

Chapter 1

The Significance of Irvine - A Possible Analogue of a Terrestrial Tholeiite and its Petrologic Implications for Crustal Diversity on Mars

1. INTRODUCTION

On Mars, both the primary and secondary crusts are proposed to be thick, with the primary crust ranging from 10-45 km thick (although 20-30 km thick is most likely) (Norman, 1999) and the secondary crust from 27-37 km thick (derived from the nominal crustal value of 57 km (Taylor et al., 2006)). The lack of plate tectonics on Mars (Breuer and Spohn, 2003 and references therein) and its thick crust suggests that continental intra-plate volcanic regimes on Earth may provide good analogues to the igneous processes that have influenced the martian surface compositions.

1.1. Fractionation in continental intra-plate magmatic regimes on Earth

On Earth, areas of intra-plate magmatism are characterized by a wide variety of rock types ranging from tholeiitic and picritic basalts to evolved rhyolites and phonolites (Figure 1.1) (e.g., Carmichael, 1964; Abbott, 1969; Frey et al., 1991; Frost et al., 1993). The wide variety of rock compositions was traditionally interpreted to reflect differing mantle source regions, differing degrees of partial melting, and differing extents of crustal contamination. However, Nekvasil et al. (2000, 2004) observed that most of the intra-plate magmatic diversity, as defined by variable bulk compositions of lavas, fell into only a few individual trends (Figure 1.2). These studies allowed for the speculation that these trends might reflect the compositional variation of liquids residual to partial

crystallization that separated from the solid residue and ascended to shallower levels (as indicated schematically in Figure 1.3).

Nekvasil et al. (2000, 2004) observed three main trends leading from silica-saturated to silica-oversaturated rocks and one primary trend leading to silica-undersaturated rocks (labeled 1-4, respectively). The first silica-saturated trend, the ocean island tholeiitic series, contains bulk rock compositions that stay within the subalkalic regime, never crossing the Irvine-Baragar Line (the line that defines the subalkalic versus alkalic fields) (Irvine and Baragar, 1971). The rocks formed within this trend range from olivine tholeiite - basaltic andesite - andesite -dacite - sodic rhyolite. The second silica-saturated trend, the potassic silica-saturated series, contains bulk rock compositions that evolve early into the alkalic regime. This trend contains sections of both silica depletion and enrichment. The silica-depletion portion of this trend extends into a low-Si, high-Fe-Ti-P ferrobasaltic rock regime. After this point, the trend starts to show silica-enrichment and joins the enrichment segment within the trachybasaltic (monzonite) zone, eventually progressing through trachyandesite (monzosyenite) - trachytes (syenites) – potassic rhyolite. The third trend, the sodic silica-saturated alkalic series, shows even more alkali enrichment. This trend evolves through sodic rhyolite. The silica-undersaturated series evolves to the highest alkali enrichment and terminates in the production of phonolite.

Experimental investigations by Spulber and Rutherford (1983), Scoates et al. (1996) and Nekvasil et al. (2004) have shown that the bulk composition trends of the silica-saturated suites can be produced by fractionation at different conditions of pressure and bulk water content. Furthermore, experiments by DiFrancesco et al. (2003), Filiberto and Nekvasil (2003) and Whitaker et al. (2007a, pers. comm.) on a continental tholeiite

from the Snake River Plain produced each of the trends of Figure 1.2 under the same conditions of pressure and water contents as was determined using a rock from each trend. The individual trends observed are as follows: Trend 1 could be produced at low pressures. The silica depletion portion of Trend 2 was produced at 9.3 kbarswith low bulk water (0.007 wt.%) and the silica enrichment trend with slightly higher water content and 5 kbars pressure. Trends 3 was produced with 2 wt.% water at 9.3 kbars. While Trend 4 was produced with the same water content as Trend 3 (2 wt.%) but at 15 kbars. Importantly, by decreasing pressure and/or water content, liquids left their original trend and began to evolve on the appropriate trend for the new conditions. Furthermore, the pressures at which the silica-saturated trends could be produced experimentally reflect fractionation at the base of the crust - at higher pressures in continental regions and at low pressures for the oceanic suites.

1.2. Fractionation in intra-plate magmatic regimes on Mars

The presence of a primary crust on Mars also suggests a density difference between the martian crust and the mantle, one that could serve as a density barrier to the ascending magmas. The importance of the density difference is evidenced on Earth's moon in that the low density of the lunar highlands impeded the rise of melt to the extent that mare basalts are only observed in deep craters (Taylor, 2001). Just as on Earth, crystallization at the crust/mantle boundary on Mars could potentially lead to a variety of evolved magmas that are compositionally quite distinct from the parent, yet not reflect differing primary mantle melts. In fact, a recent phase relation study on synthetic Humphrey composition yielded compositionally diverse residual liquids when

crystallizing at pressures corresponding to the base of the martian crust (McCubbin et al., 2008). This diversity is strongly dependent on bulk water content, with evolving liquids displaying a silica-enrichment trend with 1.7 wt.% water and a silica-depletion trend under "dry" low bulk water contents (McCubbin et al., 2008).

How much of the compositional diversity seen on the martian surface could be a result of fractionation? Answering this question is important for two primary reasons. First, the presence of such derivative liquids could lead to erroneous conclusions about the compositional character of the martian mantle based on surface igneous lithologies. Second, such a process would lead to stratification of the crust with high density cumulus minerals at the base and evolved liquids in the upper crust. Such information is important to the understanding of density profiles within the crust and the possibility of storing water at depth in the form of hydrous minerals.

On Earth the common presence of tholeiite and the recognition that it could be produced directly by partial melting of the mantle makes it a logical choice for a mantle-derived magma that could be trapped at the crust-mantle interface. This choice is not as easy to make for Mars. Yet a variety of criteria can be evaluated to make the best choice among the lithologies analyzed.

1.3. Possible martian equivalents to terrestrial tholeiite

1.3.1. *Criteria for choosing a rock*

If tholeiite on Earth can produce a wide array of rock types in continental intra-plate regions, is there a martian magma that could similarly be found in abundance that could also contribute to crustal heterogeneity during fractionation at the base of the crust?

The first criterion in identifying such a magma is that it be a "martian" composition. Since the fundamental differences between terrestrial and martian magmas are still uncertain, the most logical choice is of an actual analyzed martian composition. Although Taylor and McLennan (2009) propose, based on orbiter data, that the martian crust is tholeiitic in composition and there have been many basaltic soils analyzed by Opportunity rover (Christensen et al., 2004; Rogers and Aharonson, 2008), in order to choose a composition that could represent material directly derived from the mantle it is important to choose an actual igneous rock. Furthermore, given the signs of weathering and the mixing of the "dusty" unconsolidated material, this is the only way to verify that a composition could be igneous in nature. Therefore, the choice is best made among the igneous rocks analyzed by the MER Rover Spirit.

A second important criterion is that the rock chosen represent a liquid composition rather than one modified by accumulated crystals. This is most likely if the texture is fine-grained with no phenocrysts. If the composition is to be parental to derivative magmas, a third criterion is that it should have a sufficiently high Mg# that it could act as a parental liquid rather than a liquid at the end of a long liquid line-of-descent. However, since no one has definitively determined an acceptably primitive Mg# for martian materials (on Earth a Mg# of 72 is thought to represent a primitive magma (Winter, 2001)) the best choice is a rock that meets the first two criteria and also has the highest Mg# possible. The fourth, and last, criterion is that the chosen rock be as unaltered as possible with minimal dust on the surface.

1.3.2 *Candidates for Experimentation*

Several subalkalic and alkalic rocks encountered by the MER Rover Spirit were analyzed by APXS (Figure 1.4). Within the plains of Gusev Crater, rocks of the Adirondack class were analyzed. These have an apparent igneous texture, little alteration, and reliable compositions because most dust was removed by the Rock Abrasion Tool (RAT). The three primary rocks analyzed (Adirondack, Mazatzal, and Humphrey) are picrobasalts, have Mg#'s ranging from 50-54 and straddle the Irvine-Baragar line (Gellert et al., 2006). However, mini-TES analyses indicate high megacrystic olivine abundances (McSween et al., 2006b). Since picritic rocks on Earth often contain accumulated olivine (Carmichael et al., 1974), the presence of these megacrysts makes it difficult to be certain that the bulk composition represents a liquid.

Rocks of the Wishstone and Backstay classes were encountered during the ascent of Husband Hill (McSween et al., 2006a; Squyres et al., 2006). These rocks have highly variable textures. Wishstone, Champagne and Backstay may represent the least altered of these classes of rocks; however, all are very alkali-rich which suggest evolved liquids. Furthermore, Wishstone and Champagne have textures similar to pyroclastic tuffs. This suggests the possibility of gravitational sorting and therefore, non-liquid bulk compositions.

The Irvine class of rocks is found on the summit of Husband Hill, the highest hill within the Columbia Hills (Figure 1.5). Rocks with Irvine bulk composition appeared in a linear arrangement on the surface and were therefore thought to represent outcrops of a lava flow or dike rather than just float (Figure 1.6 and 1.7). Irvine has a fine-grained nature (Figure 1.8), is relatively unaltered and unweathered based on its APXS analysis

(reaffirmed by the low sulfur and halide contents on its surface) (McSween et al., 2006a). Compositionally, it is a mildly alkalic olivine tholeiite (based on the alkalic/subalkalic boundary of MacDonald and Katsura, 1964) and with a Mg# of 54 it fulfills all of the criteria mentioned above and is a reasonable choice for a martian mantle derived tholeiite.

2. EXPERIMENTAL/ANALYTICAL PROCEDURE

2.1 Strategy

In order to properly assess the possible range in melt compositions that could arise from a parental liquid of Irvine composition crystallizing near the base of the martian crust, a range of variables were taken into account. Crystallization experiments were performed over a range of temperatures, at 9.3 kbars(~70 km depth), under both hydrous and nominally anhydrous conditions. These experiments were run in graphite capsules which yielded an fO_2 at this pressure of ~1.5-2.5 log units below FMQ - a reasonable oxygen fugacity for martian magmas (Karner et al., 2007). The abundances of each phase, and of the bulk solids, were computed by mass balance and provide information about the amount of each type of liquid that could be added to the surface and the amount of cumulus material that could be added to the lower crust.

2.2 Experimental Procedure

2.2.1 *Starting Materials*

A synthetic mixture of the composition of Irvine (McSween et al., 2006a) was created by mixing oxides and Fe^0 powders sequentially by volume, starting with the

oxide components in smallest abundance and eventually adding in those oxides comprising larger proportions of the composition. The mixture was ground in an automated agate mortar/pestle for 3.5 hours. The $Fe^{3+}/\Sigma Fe$ value is 0.16 based on the proportion of Fe^{3+} and total Fe (Fe^{3+} and Fe^{2+}) used in the mix. The composition of this synthetic Irvine mixture IRVsynth Dry (IRV006mr) is reported in Table 1.1. This composition was obtained using electron probe microanalysis (EPMA) of a glass made at 9.3 kbars with IRVsynth Dry.

2.2.2. *Piston-Cylinder Experiments*

"*Dry" Experiments*

For experiments run under "dry" conditions, extra caution was used to ensure that both absorbed and structurally bound water was removed from the sample. This was achieved by first loading the sample, IRVsynth Dry, into a graphite capsule, then placing the loaded capsule into a silica glass tube in the presence of a Fe^0 oxygen "getter" with a glass spacer for the purpose of separation and then drying at 800°C under vacuum for 20 minutes in a vertical tube furnace. After rapidly cooling the silica tube in a cold water bath, the capsule was removed and then loaded into a barium carbonate cell assembly (Figure 1.9 same as that described in Whitaker et al., 2007a), placed into a ½ inch piston cylinder apparatus and over-pressurized (piston out method). All of the dry experiments were conducted at 9.3 kbars (10 kbars nominal).

Once pressurized, the temperature was raised to a melting temperature of 1372°C, a value safely above the liquidus, and allowed to dwell for 2.5 hours in order to homogenize. After this time, the sample was rapidly dropped to the crystallization

temperature and left to crystallize for no fewer then 2.5 days. The temperature was controlled by a Pt-$Pt_{90}Rh_{10}$ thermocouple. Each experiment was quenched isobarically. The water content was verified to be 0.01 wt.% using Micro-Fourier Transform Infrared (FTIR) spectroscopy (details of the technique are given below).

"Wet" Experiments

A hydrous material derived from the starting material was used for all "wet" experiments. This was necessary because previous work by Nekvasil et al. (2004) determined that water added to a powdered mixture would be lost through the graphite capsule at temperatures below the melting point of the powdered mixture. The hydrous material was made by first loading distilled water into a graphite-lined Pt-capsule and then adding IRVsynth Dry powder. The lid for the Pt-capsule was welded shut and the capsule was then inserted into a talc cell assembly. The assembly was then placed into a ¾ inch piston cylinder apparatus and pressurized to 9.3 kbars (10 kbars nominally). After pressurizing, the temperature was raised to the melting temperature of 1330°C and allowed to dwell for no less than 2.5 hours before rapidly quenching isobarically. Due to the number of hydrous experiments performed, multiple batches of hydrated material were made with varying textural results. While the first hydrated material was glass, the rest were, in part, crystalline. To ensure the hydrated compositions were homogenous, each of the hydrated materials were mixed in an automated agate mortar/pestle for 3 hours. The water contents of each were measured by micro-FTIR. This hydrated material was then mixed (in an automated agate mortar/pestle for 2 hours) with IRVsynth Dry to attain the desired water content of 1.0 wt.% water (IRVsynth WetLo). An additional

mixture was made to also achieve the higher bulk water content of 2 wt.% water (IRVsynth WetHi). The water contents of these hydrated compositions were verified with Micro-FTIR and are represented in Table 1.1.

After obtaining the desired water content for the powder of the "wet" experiments, the procedure used for the crystallization experiments is nearly the same as with the experiments run under "dry" conditions. The difference occurred in the drying, in that after being loaded into the capsule, the hydrous sample was dried under vacuum at 130-150°C for 45 minutes to 1 hour to drive off absorbed water only. The starting compositions were obtained by electron microprobe (EMP) analysis of glass. As shown in Table 1.1 the compositions of the dry and wet glasses are consistent. However, there is a problem with the aluminum content of IRVsynth WetLo, in that it is higher than Irvine and the two other synthetic Irvine compositions. The origin of the excess aluminum is unknown.

Oxygen Fugacity

Finally, in order to prevent oxygen fugacity from increasing beyond the graphite-CO-CO_2 (GCO) buffer, a graphite capsule was used. While only providing an upper fO_2 limit (Eugster and Skippen, 1967), this technique yields values between 1.0 and 2.5 log units below FMQ with conditions at 9.3 kbars (Whitaker et al., 2007a). However, none of the phase assemblages present in this study were appropriate for verifying this using the QUILF calculations of Anderson et al. (1993).

2.3 Analytical Procedure

2.3.1 *EPMA Analysis*

After each experiment, a thin section of the run product was made. This was first examined optically and then carbon coated and analyzed by electron microprobe. EMPA was performed at Stony Brook University using a Cameca Camebax EMP that is equipped with four wavelength dispersive spectrometers. For the analysis, an accelerating voltage of 15 kV and a nominal beam current of 10nA were used. However due to the volatility of sodium, for Na-bearing phases the largest possible raster size and a time-zero correction were used in order to minimize unknown analytical problems that occur during highly focused electron beam analysis on sodic materials. The correction technique used by Nekvasil et al. (2004) was adopted for sodium loss. The technique consists of computing the norm of the glass and adding sodium back to the analysis just to the point where all normative corundum was replaced by normative albite.

Mass-balance calculations to obtain abundances of phases were performed using the IgPet Program Suite (Carr, 2002). These calculations were also used to ensure that the analyses were reasonable and that no phase was overlooked during microprobe analysis. The calculated mineral abundances were then used to determine the bulk solids present at each crystallization temperature.

2.3.2. *Micro-FTIR Spectroscopy*

In order to determine the water content of both the hydrous glasses and of the melting and crystallization runs, infrared spectroscopic measurements were conducted on the experimental glass products. These analyses were conducted at room temperature in

transmittance mode with a Thermo Nicolet 20SXB FTIR spectrometer at Stony Brook University. The IR spectra were collected from doubly polished wafers (20 – 50 μm thick) of the run products over the mid-IR (1400-4000 cm^{-1}) to near-IR regions (3700-6500 cm^{-1}) using a KBr beam splitter, narrow range Mercury Cadmium Telluride (MCT/A) detector, and globar source. Before data collection, both the spectrometer and the IR objective were purged with dry nitrogen gas at a rate of 15 1/min. The water content was measured in total dissolved water concentrations and was determined for each glass from the intensity of the broad band at 3570 cm^{-1} following the calculation scheme of Mandeville et al. (2002). Approximately 1024 scans were performed for each IR spectrum acquired at a resolution of 4 cm^{-1}. Before each analysis, the point at which the beam would be focused was examined optically to ensure that only glass was being measured. For runs with non-zero crystalline phase abundances, the computed mineral abundances and measured water contents of the glass were used to compute the original bulk water content.

3. RESULTS

3.1. "Dry" Experiments at Depth (9.3 kbar)

Crystallization experiments run under "dry" conditions were kept at 9.3 kbars throughout the entire sequence of melting, crystallization, and quench. The temperature range for these experiments was from 1300-1050°C with the starting water content at 0.01 wt.% water. The liquidus temperature appears to be just above 1300°C; the solidus temperature is below 1050°C.

3.1.1. *Mineral Phases*

The mineral phases and their respective compositions for each temperature are listed in Table 1.2a; the abundance of each phase is shown in Figure 1.10 and can also be found in Table 1.3. At the crystallization temperature of 1300°C, forsteritic olivine was present and comprised less then 4 % of the total volume. The next mineral phases to appear are pigeonite and Cr-spinel at 1200°C. For these experiments, the pyroxenes generally have been classified on the basis of their Ca contents (by means of their Wo classification) as follows:

Wo content (wt.%)
Orthopyroxene ≤ 4
$4 <$ Low Ca-Pigeonite < 6
$6 \leq$ Pigeonite < 18
$18 \leq$ High Ca-Pigeonite (Subcalcic Augite) < 25
Augite ≥ 25

At 1200°C glass is still the dominant phase, with olivine having the highest mineral abundance. At 1170°C olivine and pigeonite are the only mineral phases present; however pigeonite is the more abundant mineral phase. At 1136°C olivine and pigeonite were still present and plagioclase made its first appearance. The crystallization at 1050°C yielded many mineral phases. In addition to the pre-existing mineral phases, subcalcic augite, ilmenite and apatite also formed. The formation of apatite is interesting since this was a nominally anhydrous crystallization experiment, however due to the isolated pockets of the residual liquid in the run product at this temperature and given the accumulation of water in the residual liquids, it is possible that the water content in some of the liquid pockets was quite high. With the exception of spinel at 1200°C, once a mineral phase entered the assemblage it was present throughout the entire range of

temperatures. The compositions of the ferromagnesian phases are projected in Figure 1.11 and the evolution of the bulk solids is represented in Table 1.4 and Figure 1.12.

3.1.2. *Liquid Evolution*

Table 1.2b and Figure 1.12 indicate the compositional evolution of liquids residual to crystallization. As seen in Figure 1.12 the residual liquids initially follow a silica-enrichment trend that eventually diverges into a silica-depletion trend with an apparent and steady enrichment in Ti, P, K and to a lesser degree Ca with decreasing temperature. The Fe content initially shows a depletion trend, but with the crystallization of plagioclase at 1136°C an abrupt enrichment in Fe occurs within the liquid. At 1100°C the Fe content also increases and therefore Fe-enrichment is likely to continue with increased crystallization. Mg is the only element that progressively decreases within the liquid while Na and Al began showing an enrichment trend but eventually decrease once plagioclase crystallized. The glass analyzed at the lowest-temperature crystallization experiment (1050°C) appears inconsistent with the higher temperature trend. At this temperature, however, glass is found only in isolated pockets and may be out of equilibrium.

3.2. "Wet" Experiments at Depth (9.3 kbar)

Crystallization experiments run under "moderately wet" and "wet" conditions were kept at 9.3 kbars throughout the entire sequence of melting, crystallization and quench. The temperature range for the "moderately wet" experiments was from 1150-1050°C with the starting water content at 1.0 wt.% water. The temperature range for the

"wet" experiments was from 1200-940°C with the starting water content of 2.0 wt.% water. The liquidus temperature for the crystallization experiment of Irvine performed under "moderately wet" conditions (1.0 wt.% H_2O) lies above 1200°C and could be as high as 1250°C; the solidus temperature is below 1050°C. The liquidus temperature for the crystallization experiment of Irvine performed under "wet" conditions (2.0 wt.% H_2O) is likewise above 1200°C and may be as high as 1225°C; the solidus temperature is below 940°C.

3.2.1. *Mineral Phases*

Intermediate Water Content (1.0 wt.% H_2O)

The mineral phases and their respective compositions for each temperature can be found in Table 1.5a and the abundance of each phase is represented in Figure 1.13 and found in Table 1.6. At the crystallization temperature of 1150°C there are three mineral phases present, forsteritic olivine, orthopyroxene and spinel, with orthopyroxene being the most abundant mineral phase. Pigeonite and plagioclase first appear at 1100°C and at the lowest crystallization temperature of 1050°C, orthopyroxene is no longer present; olivine and pigeonite are still present but in different proportions. At 1050°C the spinel has also been replaced by magnetite. The compositions of the ferromagnesian phases are projected in Figure 1.14 and the evolution of the bulk solids is given in Table 1.7 and Figure 1.15.

Higher Water Content (~2.0 wt.% H_2O)

The mineral phases and their respective compositions for each temperature are listed in Table 1.8a; and the abundance of each phase is represented in Figure 1.16 and can be found in Table 1.9. At the crystallization temperature of 1200°C there are two mineral phases present, forsteritic olivine and Cr-spinel. At the next crystallization temperature of 1150°C the same mineral phases are present, though in different proportions with olivine comprising a much greater percent by weight. Another difference between the two crystallization temperatures is the size of the Cr-spinel grains, with the once large spinel grains greatly decreasing in size. At 1100°C, along with olivine and Cr-spinel, orthopyroxene is present and then at 1050°C, with the aforementioned mineral phases persisting, pigeonite and augite were crystallized. However, due to its ragged appearance and its presence in cores only, the augite seems to be unstable. Although not thought to be a stable phase, the augite could not be ignored in the mass balance computations due to its significant abundance.

At 1000°C, spinel is no longer observed and Ti-amphibole is present. As was the case with augite at 1050°C, the augite seen at this temperature is ragged, indicating that it is not stable; but again, due to its abundance, augite could not be ignored in the mass balance calculations. At the crystallization temperature of 980°C olivine, orthopyroxene, pigeonite and Ti-amphibole are still present. Apatite is the new phase at this temperature, which persists throughout the rest of the crystallization temperatures. Although the apatite grains were often too small for accurate EPMA, their presence was verified with Energy Dispersive Spectrometry (EDS). The same mineral phases that are present at 980°C are also present at 960°C, though in different proportions. At the lowest

crystallization temperature of 940°C the mineral phases olivine, orthopyroxene, Ti-amphibole and apatite are present. It is important to note that with the entrance of Ti-amphibole at 1000°C, this mineral phase quickly dominated the regime, eventually representing more than half of the bulk solids. The compositions of the ferromagnesian phases are projected in Figure 1.16 and the evolution of these bulk solids is represented in Table 1.10 and Figure 1.17.

3.2.2. *Liquid Evolution*

Intermediate Water Content (1.0 wt.% H_2O)

Table 1.5b and Figure 1.15 represent the compositional evolution of the liquids residual to crystallization. As can be seen in Figure 1.15, the residual liquids initially follow a silica-enrichment trend that eventually diverges into a silica-depletion trend with an apparent and steady enrichment in Ti, P, K, and to a lesser degree Na. The Fe content initially shows a depletion trend, but with the crystallization of plagioclase at 1100°C the trend stabilizes. It is possible that upon further crystallization this will turn into a Fe-enrichment trend like that seen in crystallization experiments under "dry" conditions. Mg is the only element that decreased steadily within the liquid while Al and Ca began showing an enrichment trend but eventually began to be depleted once plagioclase crystallized.

Higher Water Content (~2.0 wt.% H_2O)

Table 1.8b and Figure 1.17 indicate the compositional evolution of the liquids residual to crystallization. As can be seen in Figure 1.17, the residual liquids follow a

silica-enrichment trend with a steady depletion in Mg and Fe. Many oxide components are greatly affected by the entrance of Ti-amphibole, with Ti and K initially increasing and then steadily decreasing.

4. DISCUSSION

The results of the experiments indicate that liquids arising from fractionation of an Irvine-like tholeiite at 9.3 kbars remain basaltic in silica content at least through 83% crystallinity for "dry" and 72% crystallinity for 1.0 wt.% water; never attaining silica contents of 50 wt.% or higher in spite of the Mg# trending towards 30 (Figure 1.18 and Table 1.5b). These liquids evolve primarily by alkali enrichment at almost constant silica, extending into the alkalic field. At late stages, the liquids show silica depletion and are alkalic, entering the hawaiitic field, yet remain silica-saturated (hypersthene in the norm). These liquids are characterized by high Ti and P contents. Although initially the total Fe content increases, it eventually falls back to values similar to the starting composition in spite of the low Mg#s.

At 2.0 wt.% bulk water, the amount of silica-enrichment of the residual liquids is extensive, extending the liquids through the trachyandesite field towards rhyolite. This silica-enrichment is primarily due to extensive olivine crystallization early followed by amphibole crystallization. This is coupled with alkali and alumina enrichment and iron depletion.

4.1. Difference in composition between synthesized starting materials

Although not thought to be different enough to change the mineral assemblages crystallized and therefore the liquid evolution, there is a marked difference in the starting compositions between IRVsynth Dry and IRVsynth WetLo. While the definitive origin for the difference is unknown, since IRVsynth WetLo was derived directly from IRVsynth Dry, the difference can be attributed to possible heterogeneity or foreign matter. It is also possible that, since the differences are small and some quite minute, they could actually be attributed to EPMA error.

The subtle variation in composition does not effect the crystallization because where the small differences occur, in that the differences are not crucial in determining the mineral phases to be crystallized. This is evident, in part, due to the similarity between the "dry" and "moderately wet" residual liquid trends and due to the minerals that actually crystallized. While different minerals are crystallizing, the phases are similar in that they are pyroxenes and it is because of this that the trends are similar.

4.2. Comparisons with residual liquids from other parental magmas

4.2.1. *Comparison with terrestrial tholeiite evolution*

Equilibrium crystallization experiments performed by Whitaker et al. (2007a) on a terrestrial olivine tholeiite at 9.3 kbars and under nominally anhydrous conditions (< ~0.05 wt.% water) are shown in Figure 1.19 and 1.20, respectively, depicting the compositional evolution of the liquids residual to crystallization and phase abundances. As is the case with Irvine, under nominally dry conditions, the silica content of derivative liquids of the terrestrial tholeiite remains basaltic even to about 7 wt.% liquid remaining

in the system (Whitaker et al., 2007a). Late-stage liquids for both show silica depletion as the residual liquids evolve to higher alkali, titania, and phosphoria concentrations and lower magnesia. Both starting materials produce alkalic residual liquids while remaining silica-saturated.

There are some significant differences between the terrestrial tholeiite used by Whitaker et al. (2007a) and the Irvine composition used here. These differences result in different mineral assemblages and hence, differences in liquid lines-of-descent. The terrestrial tholeiite chosen by Whitaker et al. (2007a) has approximately twice the CaO content, and roughly half of the FeO_T of Irvine (Table 1.11). So, while both rocks appear to have forsteritic olivine on the liquidus, the olivine crystallized with Irvine composition is more Fe-rich than that of the terrestrial olivine at a similar degree of crystallinity (and temperature). Furthermore, given the dramatically higher calcium content of terrestrial olivine tholeiite, it is not unexpected that augite (high-Ca pyroxene) crystallizes early from the terrestrial tholeiite, while pigeonite (moderate-Ca pyroxene) is the first pyroxene to form from the Irvine composition. Augite does not crystallize from the "dry" Irvine composition until >80% crystallinity is attained. Instead, pigeonite is the dominant pyroxene. Similarly, the higher calcia in the terrestrial tholeiite may have contributed to earlier crystallization of plagioclase and hence alumina depletion in the derivative liquids of the terrestrial tholeiite. The lower alumina content of the bulk Irvine composition may also have played a role in suppressing plagioclase crystallization. The late appearance of plagioclase in the melts residual to Irvine crystallization would permit an increase in alumina to extend to lower temperatures than for the terrestrial tholeiite.

Unlike the trends of other oxide components, which contain internal differences, the evolution of potassia, titania and phosphoria are quite similar. Figure 1.19 shows the consistent enrichment in these melt constituents throughout the liquid evolution for both the terrestrial and proposed martian tholeiite. The steady increase in composition is due to the lack of significant mineral formation containing sufficiently high concentration of all three oxides. In fact, for both rock compositions the percent of each constituent at least doubles by the time 65 wt.% crystallinity is achieved.

When comparing the liquid evolution of Irvine under "wet" conditions to the silica-saturated compositional trends that are seen on Earth (Figure 1.2), the similarities and differences between the evolutionary paths of terrestrial tholeiite and the proposed martian tholeiite are evident. The most obvious of the differences are, again, related to the higher iron content of Irvine. While alkalis quickly enrich in the liquid evolution for terrestrial tholeiites and for Irvine under "dry" conditions, crystallization experiments performed on Irvine under "wet" conditions show the liquid enriching in SiO_2 while the alkalis generally stagnate; staying in the subalkalic field until a pyroxene is able to dominate the residual liquids. It is only after Irvine crystallized amphibole that this "wet" martian trend became similar with the terrestrial trend, with the residual liquids "hugging" the Irvine-Baragar line within the alkalic field as is seen with the potassic silica-saturated alkalic series on Earth (Figures 1.19 and 1.2). This corresponds nicely with the premise of this research in that this series is found exclusively in continental regimes where there are hot-spot related igneous provinces (Whitaker et al., 2007a).

4.2.2. *Comparison with liquids produced by crystallization of Humphrey*

The Gusev Crater picrobasalt Humphrey has been considered by some to represent a mantle-derived melt (Monders et al., 2007). If Irvine is a martian analog of a terrestrial tholeiite it would also represent a mantle-derived melt that has undergone little modification during ascent to the surface. In this case, comparison of the phase relations of these two rocks and identification of similarities will help define "martian mineralogies" and could illustrate the important role that the starting composition plays in the evolution of a liquid. Humphrey and Irvine have similar SiO_2 and FeO_T contents, but Humphrey is lower in K_2O and MgO than Irvine. Furthermore, Humphrey has higher Na_2O and Al_2O_3 contents and a significantly higher CaO content.

Just as for Irvine, bulk water content plays an important role in dictating liquid evolution of a magma of Humphrey composition. Under "dry" conditions, both rock compositions produce the same mineral assemblage with the exception of chromite (Humphrey, McCubbin et al., 2008) and ilmenite (Irvine, this work) (Figure 1.23). However, the lower MgO, higher Al_2O_3 and CaO content of Humphrey stabilizes pigeonite and plagioclase at higher temperatures than in Irvine composition magmas. These minerals cause liquids residual to Humphrey to start undergoing silica-depletion at an earlier stage of crystallization than Irvine. The high plagioclase abundance further causes the stronger iron enrichment of the Humphrey residual liquids relative to Irvine (Fig. 2.16) in spite of the similarities in bulk FeO contents of the two rocks.

The liquid line of descent is even more similar between Humphrey and Irvine at the highest water contents of each set of experiments, 1.7 wt.% H_2O for Humphrey (McCubbin et al., 2008) and 2.0 wt.% water for Irvine (Fig. 1.20). Both rock

compositions start with olivine crystallization followed by olivine, orthopyroxene and with pigeonite appearing next in the sequence. They both eventually crystallize the assemblage olivine, pigeonite, augite and amphibole before olivine disappears from the Humphrey assemblage and plagioclase appears. At 74 % crystallinity, plagioclase has not yet appeared in Irvine with 2.0 wt.% water and olivine remains in the assemblage. These differences, however, do not cause major changes in the liquid lines-of-descent.

Since the water content of the "wet" experiments performed on Humphrey composition nearly splits the range in the water contents of the "wet" and "moderately wet" experiments performed on Irvine composition, it is important to also compare Humphrey "wet" to Irvine "moderately wet". The main point of deviation between Humphrey Wet and Irvine WetLo is that unlike in Humphrey, which shows a clear Si-enrichment trend, Irvine WetLo shows a Si-depletion trend similar to that seen under "dry" conditions. The cause of the Si-enrichment trend can be linked to the crystallization of an amphibole phase, which is a mineral with a low Si-content relative to the other phases present in the system. The amphibole phase that crystallized in experiments performed with a Humphrey starting composition is a high-Ca amphibole. It can be speculated that due to the similarities between the original compositions and the pattern of crystallization up to the point where amphibole was crystallized, that the amphibole that would be stable in the Irvine assemblage would have been the same, or similar, Ca-bearing amphibole. Therefore, it is because of the low(er) calcium content in Irvine that the silica enrichment trend does not occur. This hypothesis was reaffirmed by the high-Ca amphibole that crystallized under "wet" conditions.

Irvine and Humphrey compositions have many similarities, yet also some important differences. Although compositionally similar in a variety of constituent oxides, Figure 1.20 shows that Humphrey cannot produce Irvine under the conditions of the experiments presented by McCubbin et al. (2008) since Irvine does not lie on either of the two Humphrey liquid lines of descent. Similarly Irvine cannot produce Humphrey based on the experimental conditions of this study. With such similarities yet having no reasonable evolutionary relationship, is it possible that they both could represent different types of martian mantle material? It is known that the martian mantle is heterogeneous (Zimbelman et al., 1991) in terms of bulk mineralogy and, without the mixing caused by subducting lithosphere, may well be stratified. Therefore, theoretically, both of these rock compositions could have been derived from different layers within the mantle. Or in other words, they could be mantle melts that were derived from different source regions. If both are from the mantle, this would mean that martian tholeiite is a non-unique composition and the concept of "finding the martian equivalent to the terrestrial tholeiite" is not-useful. This is because melting from different portions of the mantle will yield significant variations in major element chemistry and/or the resulting melts. Consequently, Mars may display an even greater range in rock types than are even observed on Earth.

4.3. Relationship to other rocks analyzed by the MER Rover Spirit

Backstay

The experimental residual liquids can also be used to assess the possibility of a simple fractionation relationship between Irvine and other Gusev Crater rocks with lower

Mg#'s. Focusing on rocks with non-cumulate textures, the rock Backstay meets the criteria of likely representing a liquid based on textural evidence and being more evolved than Irvine. Figure 1.18 and Table 1.2b shows that the residual liquid at 1170°C from "dry" Irvine magma matches the SiO_2, Na_2O, K_2O, and P_2O_5 of Backstay. Backstay is slightly lower in FeO_T, however, and significantly lower in CaO, TiO_2 and Al_2O_3. The liquids residual to crystallization of Irvine with 2.0 wt.% water matches the silica content of Backstay at 1150°C (Figure 2.14 and Table 1.8b). This liquid gives a better agreement with TiO_2, Al_2O_3, MgO and CaO, than the dry liquid at 1170°C. However, it provides a worse fit for the alkalis and P_2O_5. The residual liquid at this temperature is also significantly higher in FeO_T than Backstay. Based on this comparison, Backstay cannot be readily derived from an Irvine parent with the water contents of these experiments through fractionation at the base of a thick martian crust.

Wishstone

The Wishstone class of rocks found on Husband Hill contains rocks that may represent liquids, although texturally (McSween et al., 2006a) they more likely represent welded tuffs than lava flows. The rock Wishstone of the Wishstone class (shown in Figure 1.1 and 1.22), is a relatively more evolved rock. More specifically, it is depleted in silica and magnesia and enriched in titania and phosphoria. Previous studies performed on martian rock compositions (i.e. Humphrey from McCubbin et al. (2008) and Backstay from Nekvasil et al. (submitted)) demonstrate a liquid trend toward some of the oxide components of Wishstone. A magma of Humphrey composition can readily produce the

SiO_2, Na_2O and K_2O, MgO and CaO of Wishstone at 1120°C but such liquids are too low in TiO_2, Al_2O_3, P_2O_5 and too high in FeO_T.

The liquid evolution of Irvine under "moderately wet" conditions (1.0 wt.% H_2O) demonstrates a trend towards a composition that is the best match to date for the composition of Wishstone, as seen in Figures 1.19 and 1.22 since there is still Si- and Fe-depletion with Ti- and P- enrichment. Although, it must be stated that the trend towards Wishstone will not produce an exact match, the presence of this Fe-depletion trend is promising.

4.4. Implications for martian crustal evolution

If the composition of Irvine represents a common mantle-derived melt on Mars, and the martian crust presents a density barrier to ascent of Irvine-like magmas, then ponding and crystallization at depth would produce a variety of residual liquids whose compositions differ strongly from the original Irvine composition. Although some workers (Dreibus and Wänke, 1985, 1987; Mysen et al., 1998) concluded that the martian mantle is low in water, recent results based on the studies of martian meteorites (e.g., Elardo et al., 2008; McCubbin et al., In prep) suggest that the martian mantle had significant water contents. However, unlike on Earth where subduction re-hydrates the terrestrial mantle, it is likely that magmas on Mars became drier with time. This would imply that early production of the secondary crust would have involved adding silica-rich residual liquids to the surface or near-surface and underplating of the primary crust with an olivine-rich cumulate material with low SiO_2 and CaO contents and high MgO and FeO (Table 1.10). Magmas not reaching the surface could crystallize amphibole and

therefore leave a water-rich residue that could lead to partial melting of the crust at a later time.

As the magmatic source region became de-hydrated, the cumulate material underplating the crust would be olivine- and pigeonite-dominated. The evolved magmas reaching the surface would more commonly be basaltic, and with increased evolution reach low silica contents. This "new" evolved and silica depleted magma would cover the "older" silica rich magmas (Figure 1.24). In this way, the martian crust could have significant compositional heterogeneities. This hypothesis seems to be supported by both rover and orbiter data.

Christensen et al. (2005) noted evidence for crustal compositional diversity on Mars in the presence of high-silica dacite in Syrtis Major caldera. This observation supports the possibility that basalts cover a silica-rich crust which could also contribute to providing a density barrier for rising mantle-derived magmas. Furthermore, given the high water content needed to cause the residual liquids of Irvine composition to trend towards silica enrichment, it is likely that the silica-rich portion of the secondary crust is thin relative to the basaltic crust overlaying it. It must be noted that McCubbin et al. (2008) achieved silica rich residual liquids with lower water contents, due to the relatively high calcium content in the original composition which allowed the crystallization of amphibole before plagioclase. However, given that the calcia content of proposed mantle compositions is ~ 2.5 wt.% (Dreibus and Wänke, 1985; Bertka and Fei, 1998), and that this would be concentrated to ~ 6 wt.% in the upper mantle, it is probable that Irvine composition would be more prevalent. In which case, the diversity proposed by McCubbin et al. (2008) might only be relevant to mantle melting of Humphrey like

compositions when water contests are high (>1.0 wt.%). For that reason, if starting compositions drive the importance of water content, and similar water contents allow for silica enrichment of residual liquids in one tholeiite but not the other, then it may explain why basalts dominate the martian surface.

Table 1.1. Composition of Irvine (Unbrushed) and Irvine after SO_3 adjustment from McSween et al. (2006a), with Irvine (VF) recast from Irvine on a volatile free basis. EPMA of fused synthetic mixes of Irvine composition with 0.01 wt.% bulk water (IRVsynth Dry), 1.0 wt.% bulk water (IRVsynth WetLo), and 2.0 wt.% bulk water (IRVsynth WetHi). Water contents were determined by micro-FTIR.

Oxide	Unbrushed Irvine*	Irvine*	Irvine (VF)	IRVsynth Dry‡	IRVsynth WetLo‡	IRVsynth WetHi‡
SiO_2	47.0	46.6	47.30	46.86	45.61	46.29
TiO_2	1.06	1.05	1.07	1.04	1.01	0.99
Al_2O_3	10.6	10.5	10.66	10.45	11.84	9.94
Fe_2O_3	7.68	7.61	n.d.[a]	n.d.[a]	n.d.[a]	n.d.[a]
Cr_2O_3	0.2	0.2	0.20	0.22	0.18	0.25
FeO	12.3	12.2	n.d.[a]	n.d.[a]	n.d.[a]	n.d.[a]
FeO_T	n.d.[a]	n.d.[a]	19.33	18.81	17.79	18.38
MnO	0.36	0.36	0.37	0.39	0.32	0.39
MgO	10.6	10.5	10.66	10.28	10.08	10.25
CaO	6.03	5.98	6.07	5.62	5.29	5.54
Na_2O	2.68	2.66	2.70	2.73	2.50	2.51
K_2O	0.68	0.67	0.68	0.69	0.65	0.62
P_2O_5	0.97	0.96	0.97	0.97	0.92	1.00
SO_3	2.37	0.75	n.d.[a]	n.d.[a]	n.d.[a]	n.d.[a]
Cl	0.45	0.00	n.d.[a]	n.d.[a]	n.d.[a]	n.d.[a]
Total	103.0	100.0	100.0	98.06	96.20	96.16
Mg#[b]	54	54	54	53	50	54
H_2O in synthetic glass (wt. %)				0.01[c]	1.0[c]	1.93[c]

* McSween et al (2006a)

‡ Synthetic composition used for this study

[a] Not analyzed

[b] Mg# = Molar Mg/(Mg + Fe^{2+}) assuming an Fe^{2+}/Fe_{Tot} ratio of 0.85.

[c] Measured by FTIR (not included in total).

Table 1.2a. Compositions of co-existing minerals as a function of temperature for IRVsynth Dry (0.01 wt.% bulk water [a]) at 9.3 kbars.

Phase	**Olivine**						**Spinel**	**Pigeonite**
Experiment #	IRV012dr	IRV005dr	IRV005dr	IRV013dr	IRV011dr	IRV010dr	IRV005dr	IRV005dr
Temperature (°C)	1300	1250	1200	1170	1136	1050	1200	1200
SiO_2	36.71	37.53	35.81	35.63	34.20	35.04	2.62	50.82
TiO_2	0.02	0.02	0.04	0.05	0.05	0.15	1.68	0.28
Al_2O_3	0.07	0.08	0.06	0.08	0.05	0.88	18.64	2.84
Cr_2O_3	0.14	0.20	0.14	0.07	0.06	0.06	37.09	1.02
FeO	25.29	26.43	31.83	35.08	39.72	41.47	28.40	19.30
MnO	0.40	0.42	0.49	0.50	0.56	0.58	0.32	0.45
MgO	35.75	36.00	30.79	26.97	24.42	20.52	7.25	21.01
CaO	0.19	0.21	0.29	0.38	0.29	0.47	0.26	3.17
Na_2O	0.03	0.02	0.03	0.00	0.02	0.35	0.00	0.08
K_2O	0.01	0.00	0.00	0.00	0.01	0.06	0.01	0.00
P_2O_5	0.25	0.30	0.19	0.12	0.11	0.26	0.03	0.07
Total	98.86	101.21	99.65	98.89	99.48	99.84	96.30	99.04
Phase Comp. (mol %)	$Fo_{71}(La_{0.27})$	$Fo_{71}(La_{0.30})$	$Fo_{63}(La_{0.43})$	$Fo_{57}(La_{0.58})$	$Fo_{52}(La_{0.44})$	$Fo_{40}(La_{0.38})$	$Ul_4Mt_8Hy_{38}Cr_{50}$	$En_{61}Wo_8Fs_{31}$

Phase	**Pigeonite**			**Plagioclase**		**Subcalcic Augite**	**Ilmenite**
Experiment #	IRV013dr	IRV011dr	IRV010dr	IRV011dr	IRV010dr	IRV010dr	IRV010dr
Temperature (°C)	1170	1136	1050	1136	1050	1050	1050
SiO_2	50.68	48.61	50.94	57.97	57.64	44.63	2.81
TiO_2	0.50	0.73	0.92	0.10	0.15	1.23	47.45
Al_2O_3	4.38	4.99	4.99	25.67	23.51	5.87	0.86
Cr_2O_3	0.70	0.64	0.30	0.03	0.01	0.16	0.97
FeO	18.75	20.70	22.12	0.74	1.68	19.57	41.86
MnO	0.49	0.44	0.58	0.00	0.04	0.48	0.42
MgO	18.12	16.69	14.64	0.05	0.90	13.03	4.23
CaO	5.29	5.23	4.22	7.69	6.32	11.64	0.60
Na_2O	0.23	0.34	0.89	6.63 (6.86*)	5.80 (6.50*)	0.67	0.18
K_2O	0.02	0.05	0.16	0.70	1.67	0.05	0.02
P_2O_5	0.12	0.21	0.28	0.15	0.20	1.15	0.04
Total	99.28	98.64	100.05	99.72	97.91	98.46	99.43
Phase Comp. (mol %)	$En_{54}Wo_{15}Fs_{31}$	$En_{50}Wo_{16}Fs_{34}$	$En_{43}Wo_{20}Fs_{37}$	$Ab_{58}An_{38}Or_4$	$Ab_{57}An_{33}Or_{10}$	$En_{53}Wo_{18}Fs_{29}$	$Ilm_{91}Hem_9$

[a] measured by FTIR.

* Value corrected for Na-loss, corrected value is listed parenthetically

Table 1.2b. Compositions of glass as a function of temperature for IRVsynth Dry (0.01 wt.% bulk water [a]) at 9.3 kbars.

Experiment	IRV012dr	IRV004dr	IRV005dr	IRV013dr	IRV011dr	*IRV010dr* [/]
Temperature (°C)	1300	1250	1200	1170	1136	*1050*
SiO_2	47.58	48.11	48.71	48.69	44.94	*55.22*
TiO_2	1.13	1.12	1.34	1.43	2.26	*0.23*
Al_2O_3	10.83	11.33	13.06	15.15	12.61	*19.61*
Cr_2O_3	0.18	0.17	0.10	0.03	0.07	*0.06*
FeO	18.79	18.43	17.21	15.37	18.29	*3.86*
MnO	0.36	0.36	0.35	0.29	0.33	*0.10*
MgO	9.28	8.83	5.99	4.29	4.01	*2.06*
CaO	5.86	6.04	6.75	7.02	7.07	*5.62*
Na_2O	2.49	2.75	3.54	4.10	3.82	*5.64*
K_2O	0.70	0.75	0.86	1.06	1.34	*1.58*
P_2O_5	0.98	1.05	1.30	1.50	2.41	*0.26*
Total	98.16	98.92	99.20	98.93	97.16	*94.26*
Mg# [b]	51	50	42	37	31	*53*

[a] measured by FTIR.

[b] Mg# = Molar Mg/(Mg + Fe^{2+}) assuming an Fe^{2+}/Fe_{Tot} ratio of 0.85.

[/] Small pockets of glass- not suitable for interpreting residual liquid evolution.

Table 1.3. Computed phase abundances at each crystallization temperature for IRVsynth Dry (0.01 wt.% bulk water [a]) at 9.3 kbars. Sum of the squares of the residuals (s.s.r.) is indicated for each computed assemblage.

Experiment (No.)	IRV012dr	IRV004dr	IRV005dr	IRV013dr	IRV011dr	*IRV010dr*
Temperature (°C)	1300	1250	1200	1170	1136	*1050*
Computed Mode (wt.%)	Gl 96.3 Ol 3.7	Gl 93.9 Ol 6.1	Gl 78.6 Ol 12.1 Pig 9.2 Sp 0.1	Gl 65.8, Ol 15.7 Pig 18.6	Gl 35.7 Ol 14.1 Pig 32.6 Plag 17.6	*Gl 17.1* *Ol 26.* *Pig 20.1* *Aug 11.6* *Plag 22.1* *Ilm 1.4* *Apat 1.5*
Crystallinity (wt. %)	3.7	6.1	21.4	34.2	64.3	*82.9*
S.S.R.	0.142	0.106	0.018	0.019	0.009	*0.016*
H_2O in Glass (wt. %)[b]	0.01	0.01	0.01	0.02	0.03	*0.06*

Gl: glass; Ol: olivine; Pig: pigeonite; Sp: spinel; Plag: plagioclase; OPX: orthopyroxene; Aug: augite Apat: apatite; Ilm: ilmenite amph: amphibole

[a] measured by FTIR.

[b] calculated based on degree of crystallinity assuming component increases incompatibly (value not included in total).

Table 1.4. Computed compositions of bulk solids of the mineral assemblages from computed phase abundances of Table 1.3 for IRVsynth Dry at 9.3 kbars.

Experiment (No.)	IRV012dr	IRV004dr	IRV005dr	IRV013dr	IRV011dr	IRV010dr
Temperature (°C)	1300	1250	1200	1170	1136	1050
SiO_2	37.13	37.08	42.35	44.19	48.40	45.40
TiO_2	0.02	0.02	0.15	0.30	0.41	1.30
Al_2O_3	0.07	0.08	1.36	2.44	9.60	8.68
Cr_2O_3	0.14	0.20	0.71	0.41	0.35	0.13
FeO	25.59	26.11	26.60	26.47	19.60	22.49
MnO	0.40	0.41	0.47	0.50	0.35	0.41
MgO	36.16	35.57	26.63	22.37	13.98	12.23
CaO	0.20	0.20	1.54	3.07	4.86	5.51
Na_2O	0.03	0.02	0.05	0.13	2.06*	2.18*
K_2O	0.01	0.00	0.00	0.01	0.22	0.51
P_2O_5	0.25	0.30	0.14	0.12	0.17	1.15
Total	100.00	100.00	100.00	100.00	100.00	100.00
Mg#[a]	75	71	68	64	60	53

* Value calculated from plagioclase that was corrected for Na-loss.

[a] Mg# = Molar Mg/(Mg + Fe^{2+}) assuming an Fe^{2+}/Fe_{Tot} ratio of 0.85.

Table 1.5a. Compositions of co-existing minerals as a function of temperature for IRVsynth WetLo (1.0 wt.% bulk water) at 9.3 kbars.

Phase	**Olivine**			**Orthopyroxene**		**Pigeonite**
Experiment	IRV016hr	IRV015hr	IRV017hr	IRV016hr	IRV015hr	IRV015hr
Temperature (°C)	1150	1100	1050	1150	1100	1100
SiO_2	35.75	35.62	34.46	50.93	51.40	49.85
TiO_2	0.03	0.02	0.10	0.30	0.27	0.41
Al_2O_3	0.07	0.07	0.07	4.78	4.69	4.88
Cr_2O_3	0.05	0.07	0.04	0.80	0.73	0.43
FeO	33.83	36.81	41.41	19.03	19.04	21.69
MnO	0.53	0.51	0.68	0.39	0.40	0.39
MgO	28.42	26.63	22.46	21.65	21.87	20.14
CaO	0.24	0.31	0.27	1.46	1.35	2.41
Na_2O	0.01	0.00	0.03	0.08	0.05	0.09
K_2O	0.01	0.01	0.01	0.01	0.01	0.00
P_2O_5	0.12	0.07	0.08	0.02	0.02	0.03
Total	99.05	100.13	99.59	99.45	99.82	100.40
Phase Comp. (mol %)	$Fo_{60}(La_{0.36})$	$Fo_{56}(La_{0.47})$	$Fo_{49}(La_{0.42})$	$En_{65}Wo_3Fs_{32}$	$En_{65}Wo_3Fs_{32}$	$En_{60}Wo_7Fs_{33}$

Phase	**Pigeonite**	**Plagioclase**		**Spinel**		**Magnetite**
Experiment	IRV017hr	IRV015hr	IRV017hr	IRV016hr	IRV015hr	IRV017hr
Temperature (°C)	1050	1100	1050	1150	1100	1050
SiO_2	49.06	56.70	55.45	0.00	0.68	2.74
TiO_2	0.59	0.07	0.06	1.77	1.32	20.59
Al_2O_3	4.00	27.83	28.26	28.79	39.94	7.49
Cr_2O_3	0.44	0.00	0.02	27.51	15.62	8.28
FeO	22.51	0.55	0.82	30.09	31.80	54.12
MnO	0.46	0.01	0.01	0.25	0.27	0.43
MgO	18.91	0.04	0.04	7.28	8.21	3.23
CaO	2.25	9.77	10.68	0.17	0.25	0.51
Na_2O	0.09	5.93 (6.20*)	5.07 (5.66*)	0.00	0.07	0.37
K_2O	0.00	0.37	0.39	0.01	0.03	0.09
P_2O_5	0.04	0.22	0.23	0.06	0.06	0.14
Total	98.34	101.75	101.61	95.92	98.26	98.00
Phase Comp. (mol %)	$En_{56}Wo_7Fs_{37}$	$Ab_{50}An_{48}Or_2$	$Ab_{46}An_{52}Or_2$	$Ul_4Mt_6Hy_{55}Cr_{35}$	$Ul_3Mt_7Hy_{71}Cr_{19}$	$Ul_{57}Mt_{14}Hy_{16}Cr_{12}$

* Value corrected for Na-loss, corrected value is listed parenthetically.

Table 1.5b. Compositions of glass as a function of temperature for IRVsynth WetLo at 9.3 kbars.

Experiment (No.)	IRV016hr	IRV015hr	IRV017hr
Temperature (°C)	1150	1100	1050
SiO_2	47.15	46.65	45.95
TiO_2	1.27	1.65	2.62
Al_2O_3	15.04	15.01	14.11
Cr_2O_3	0.06	0.06	0.00
FeO	15.76	14.76	14.90
MnO	0.29	0.32	0.24
MgO	4.88	3.62	3.20
CaO	7.05	7.26	7.24
Na_2O	3.36 (3.52*)	3.65	3.58 (3.81*)
K_2O	0.80 (0.86*)	0.99	1.76
P_2O_5	1.26	1.59	3.02
Total	96.9	95.54	96.61
Mg#[a]	39	34	31

* Value corrected for Na-loss, corrected value is listed parenthetically.

[a] Mg# = Molar Mg/(Mg + Fe^{2+}) assuming an Fe^{2+}/Fe_{Tot} ratio of 0.85.

Table 1.6. Computed phase abundances at each crystallization temperature for IRVsynth WetLo at 9.3 kbars. Sum of the squares of the residuals (s.s.r.) is indicated for each computed assemblage.

Experiment (No.)	IRV016hr	IRV015hr	IRV017hr
Temperature (°C)	1150	1100	1050
Mode (wt.%)	Gl 71.6 Ol 8.9 OPX 19.3 Sp 0.2	Gl 53.4 Ol 14.0 OPX 4.8 Pig 17.8 Plag 9.5 Sp 0.5	Gl 28.0 Ol 16.5 Pig 29.8 Plag 25.4 Mg 0.3
Crystallinity (wt. %)	28.4	37.8	72.1
S.S.R.	0.05	0.02	0.01
H_2O in Glass (wt. %)[a]	1.4	1.9	3.6

[a] calculated based on degree of crystallinity assuming component increases incompatibly (value not included in total).
Mineral abbreviations are as in Table 2.3.

Table 1.7. Computed compositions of bulk solids of the mineral assemblages from computed phase abundances of Table **2.6** for IRVsynth WetLo at 9.3 kbars.

Experiment (No.)	IRV016hr	IRV015hr	IRV017hr
Temperature (°C)	1150	1100	1050
SiO_2	46.07	46.32	47.85
TiO_2	0.23	0.22	0.37
Al_2O_3	3.52	8.39	11.53
Cr_2O_3	0.79	0.43	0.23
FeO	23.94	21.71	19.52
MnO	0.44	0.38	0.36
MgO	23.82	18.00	13.17
CaO	1.07	3.11	4.71
Na_2O	0.06	1.28*	2.00*
K_2O	0.01	0.08	0.14
P_2O_5	0.05	0.08	0.12
Total	100.00	100.00	100.00
Mg# [a]	68	64	59

* Value calculated from plagioclase that was corrected for Na-loss.

[a] Mg# = Molar Mg/(Mg + Fe^{2+}) assuming an Fe^{2+}/Fe_{Tot} ratio of 0.85.

Table 1.8a. Compositions of co-existing minerals as a function of temperature for IRVsynth WetHi (2.0 wt.% bulk water) at 9.3 kbars.

Phase	**Olivine**							
Experiment	IRV034hr	IRV026hr	IRV025hr	IRV028hr	IRV031hr	IRV032hr	IRV033hr	IRV035hr
Temperature (°C)	1200	1150	1100	1050	1000	980	960	940
SiO_2	36.66	37.07	36.64	35.14	33.36	34.03	33.15	32.83
TiO_2	0.01	0.01	0.05	0.05	0.12	0.15	0.06	0.10
Al_2O_3	0.03	0.03	0.05	0.02	0.14	0.23	0.06	0.08
Cr_2O_3	0.14	0.14	0.03	0.01	0.12	0.12	0.00	0.05
FeO	25.23	29.90	34.56	36.48	42.09	42.98	45.76	45.65
MnO	0.37	0.49	0.52	0.55	0.51	0.62	0.70	0.70
MgO	35.60	32.40	28.45	25.86	23.17	21.69	19.11	17.72
CaO	0.11	0.17	0.23	0.26	0.23	0.24	0.24	0.23
Na_2O	0.01	0.01	0.02	0.05	0.02	0.07	0.01	0.06
K_2O	0.01	0.00	0.01	0.00	0.01	0.03	0.01	0.03
P_2O_5	0.05	0.06	0.06	0.05	0.19	0.25	0.11	0.18
Total	98.21	100.29	100.60	98.47	99.97	100.40	99.20	97.60
Phase Comp. (mol %)	$Fo_{71}(La_{0.16})$	$Fo_{66}(La_{0.24})$	$F0_{59}(La_{0.34})$	$F0_{57}(La_{0.40})$	$Fa_{49}(La_{0.35})$	$Fo_{47}(La_{0.38})$	$Fo_{43}(La_{0.38})$	$Fo_{41}(La_{0.38})$
Phase	**Orthopyroxene**						**Augite***	
Experiment	IRV025hr	IRV028hr	IRV031hr	IRV032hr	IRV033hr	IRV035hr	IRV028hr	IRV031hr
Temperature (°C)	1100	1050	1000	980	960	940	1050	1000
SiO_2	52.57	52.21	51.08	49.98	50.37	48.91	50.66	48.46
TiO_2	0.25	0.24	0.32	0.36	0.24	0.23	0.45	1.26
Al_2O_3	2.30	1.46	1.45	3.59	2.74	3.34	2.92	5.67
Cr_2O_3	0.70	0.36	0.30	0.38	0.15	0.32	0.56	0.49
FeO	20.00	21.18	22.54	24.25	26.43	26.49	16.52	13.02
MnO	0.49	0.53	0.54	0.57	0.58	0.53	0.42	0.30
MgO	21.79	21.08	20.34	18.88	17.65	16.82	15.97	11.87
CaO	1.69	1.90	1.83	1.62	1.67	1.39	10.76	17.68
Na_2O	0.06	0.04	0.05	0.07	0.06	0.05	0.19	0.51
K_2O	0.01	0.00	0.01	0.00	0.01	0.01	0.00	0.01
P_2O_5	0.03	0.02	0.01	0.03	0.02	0.04	0.16	0.36
Total	99.88	99.03	98.48	99.72	99.92	98.13	98.61	99.62
Phase Comp. (mol %)	$En_{63}Wo_4Fs_{33}$	$En_{61}Wo_4Fs_{35}$	$En_{60}Wo_4Fs_{36}$	$En_{57}Wo_4Fs_{39}$	$En_{53}Wo_4Fs_{43}$	$En_{52}Wo_3Fs_{45}$	$En_{47}Wo_{26}Fs_{27}$	$En_{43}Wo_{32}Fs_{25}$

* Unstable mineral phase

Table 1.8a. continued.

Phase	**Pigeonite**				**Ti-Amphibole**			
Experiment	IRV028hr	IRV031hr	IRV032hr	IRV033hr	IRV031hr	IRV032hr	IRV033hr	IRV035hr
Temperature (°C)	1050	1000	980	960	1000	980	960	940
SiO_2	51.39	49.64	50.40	49.00	40.43	40.68	40.91	41.10
TiO_2	0.34	0.50	0.47	0.40	3.78	4.08	3.15	2.53
Al_2O_3	2.84	4.17	3.07	3.64	13.27	13.51	12.99	12.72
Cr_2O_3	0.52	0.39	0.39	0.24	0.47	0.60	0.39	0.31
FeO	21.09	23.16	23.40	25.41	15.98	15.80	16.07	16.56
MnO	0.45	0.47	0.51	0.53	0.22	0.24	0.25	0.31
MgO	20.35	18.96	19.11	17.94	10.69	10.93	11.39	11.28
CaO	2.38	2.06	2.40	2.06	9.88	9.99	9.22	8.36
Na_2O	0.05	0.08	0.20	0.06	2.75	2.81	2.82	2.73
K_2O	0.01	0.00	0.00	0.01	0.47	0.37	0.36	0.32
P_2O_5	0.07	0.07	0.05	0.06	0.27	0.24	0.26	0.29
Total	99.49	99.49	100.01	99.35	98.20	99.25	97.80	96.50
Phase Comp. (mol %)	$En_{59}Wo_7Fs_{34}$	$En_{56}Wo_7Fs_{37}$	$En_{56}Wo_8Fs_{36}$	$En_{54}Wo_6Fs_{40}$	$En_{40}Wo_{27}Fs_{33}$	$En_{40}Wo_{27}Fs_{33}$	$En_{42}Wo_{25}Fs_{33}$	$En_{42}Wo_{23}Fs_{35}$

Phase	**Spinel**				**Apatite**
Experiment	IRV034hr	IRV026hr	IRV025hr	IRV028hr	IRV032hr
Temperature (°C)	1200	1150	1100	1050	980
SiO_2	0.00	0.00	0.00	9.54	0.49
TiO_2	1.65	2.19	3.57	4.39	0.01
Al_2O_3	13.18	15.02	14.97	16.42	0.13
Cr_2O_3	48.25	44.21	38.64	26.43	0.00
FeO	27.56	30.27	34.09	33.76	1.44
MnO	0.29	0.31	0.30	0.37	0.13
MgO	7.40	6.40	4.97	4.37	0.25
CaO	0.07	0.17	0.19	1.23	53.23
Na_2O	0.01	0.03	0.00	0.61	0.03
K_2O	0.00	0.03	0.03	0.34	0.06
P_2O_5	0.02	0.04	0.03	0.33	43.00
Total	98.43	98.66	96.80	97.78	98.77
Phase Comp. (mol %)	$Ul_4Mt_6Hy_{26}Cr_{64}$	$Ul_6Mt_6Hy_{30}Cr_{59}$	$Ul_9Mt_8Hy_{30}Cr_{53}$	$Ul_{13}Mt_{11}Hy_{37}Cr_{40}$	n.a.

Table 1.8b. Compositions of glass as a function of temperature for IRVsynth WetHi (2 wt.% bulk water) at 9.3 kbars.

Experiment (No.)	IRV034hr	IRV026hr	IRV025hr	IRV028hr	IRV031hr	IRV032hr	IRV033hr	IRV035hr
Temperature (°C)	1200	1150	1100	1050	1000	980	960	940
SiO_2	46.31	47.05	49.30	48.61	49.96	52.21	54.59	58.24
TiO_2	1.07	1.16	1.33	1.35	1.13	0.84	0.44	0.23
Al_2O_3	10.71	11.55	13.64	14.87	16.41	17.12	17.37	16.66
Cr_2O_3	0.18	0.08	0.02	0.01	0.02	0.00	0	0.00
FeO	18.22	16.66	14.59	12.65	11.69	10.35	8.29	6.10
MnO	0.30	0.39	0.30	0.26	0.23	0.20	0.15	0.13
MgO	8.74	6.33	4.56	3.38	2.51	2.00	1.40	0.99
CaO	5.74	6.12	6.91	7.12	6.30	5.68	4.79	3.18
Na_2O	2.66	2.86	3.22	3.57	4.16 (4.84*)	4.14 (4.85*)	4.19 (5.25*)	5.08 (6.05*)
K_2O	0.69	0.73	0.89	1.01	1.16	1.25	1.57	1.99
P_2O_5	0.99	1.03	1.29	1.49	1.78	1.06	0.70	0.51
Total	95.60	93.95	96.04	94.33	95.38	94.84	93.49	93.09
Mg#[a]	50	44	40	36	31	29	26	25

[a] Mg# = Molar Mg/(Mg + Fe^{2+}) assuming an Fe^{2+}/Fe_{Tot} ratio of 0.85.

* Value corrected for Na-loss, corrected value is listed parenthetically.

Table 1.9. Computed phase abundances at each crystallization temperature for IRVsynth WetHi at 9.3 kbars. Sum of the squares of the residuals (s.s.r.) is indicated for each computed assemblage.

Experiment (No.)	IRV034hr	IRV026hr	IRV025hr	IRV028hr	IRV031hr	IRV032hr	IRV033hr	IRV035hr
Temperature (°C)	1200	1150	1100	1050	1000	980	960	940
Mode (wt.%)	Gl 95.1 Ol 4.8 Sp 0.1	Gl 85.6 Ol 14.1 Sp 0.3	Gl 75.0 Ol 20.9 OPX 3.7 Sp 0.4	Gl 65.7 Ol 21.8 OPX 3.0 Pig 3.7 Aug 5.3* Sp 0.5	Gl 49.4 Ol 15.4 OPX 5.1 Pig 15.2 Aug 7.2* Amph 7.7	Gl 43.1 Ol 15.0 OPX 3.7 Pig 18.9 Amph 18.0 Apat 1.3	Gl 33.8 Ol 11.3 OPX 8.9 Pig 16.2 Amph 28.3 Apat 1.5	Gl 26.3 Ol 10.8 OPX 20.6 Amph 40.5 Apat 1.8
Crystallinity (wt. %)	4.9	14.4	25.0	34.3	50.6	56.9	66.2	73.7
S.S.R.	0.037	0.135	0.192	0.101	0.014	0.070	0.015	0.036
H_2O in Glass (wt. %)	2.03 [a]	2.26 [a]	2.57 [c]	2.94 [c]	3.93 [c]	4.44 [c]	5.71 [c]	7.34 [c]

* Unstable mineral phase

[a] measured by FTIR.

[b] Mg# = Molar Mg/(Mg + Fe^{2+}) assuming an Fe^{2+}/Fe_{Tot} ratio of 0.85.

[c] calculated based on degree of crystallinity assuming component increases incompatibly (value not included in total).

Mineral abbreviations are as in Table 2.3.

Table 1.10. Computed compositions of bulk solids of the mineral assemblages from computed phase abundances of Table **2.9** for IRVsynth WetHi at 9.3 kbars.

Experiment (No.)	IRV034hr	IRV026hr	IRV025hr	IRV028hr	IRV031hr	IRV032hr	IRV033hr	IRV035hr
Temperature (°C)	1200	1150	1100	1050	1000	980	960	940
SiO_2	36.55	36.15	38.29	40.93	43.54	41.94	42.43	42.30
TiO_2	0.04	0.06	0.13	0.23	0.99	1.52	1.52	1.52
Al_2O_3	0.31	0.37	0.61	1.18	4.31	5.63	6.95	8.22
Cr_2O_3	1.17	1.12	0.72	0.62	0.33	0.38	0.25	0.27
FeO	25.74	29.84	32.23	30.77	26.47	25.73	24.75	23.86
MnO	0.37	0.48	0.51	0.52	0.43	0.45	0.44	0.43
MgO	35.65	31.74	26.97	23.29	18.22	16.77	15.06	13.89
CaO	0.11	0.17	0.44	2.30	4.93	5.34	6.04	6.49
Na_2O	0.01	0.01	0.02	0.08	0.53	0.99	1.26	1.58
K_2O	0.01	0.00	0.01	0.01	0.08	0.13	0.16	0.19
P_2O_5	0.05	0.06	0.05	0.07	0.17	1.12	1.15	1.25
Total	100.00	100.00	100.00	100.00	100.00	100.00	100.00	100.00
Mg#[a]	74	69	64	61	59	58	56	55

[a] Mg# = Molar Mg/(Mg + Fe^{2+}) assuming an Fe^{2+}/Fe_{Tot} ratio of 0.85.

Table 1.11. Measured compositions of surface rocks Backstay and Humphrey in Gusev Crater, synthetic compositions, and a terrestrial tholeiite for comparison with Irvine.

Oxide	Irvine	Backstay Brushed*	Backstay*	Bsynth[¥]	HRAT 1[~]	Hsynth Dry[ǂ]	Hsynth Wet[ǂ]	Terrestrial Olivine Tholeiite[C]
SiO_2	46.6	49.5	49.6	50.75	46.30	47.67	45.82	47.53
TiO_2	1.05	0.93	0.93	0.92	0.58	0.53	0.54	1.43
Al_2O_3	10.5	13.3	13.3	13.29	10.78	10.88	10.39	15.03
Fe_2O_3	7.61	3.32	3.33	n.d.[a]	n.d.[a]	n.d.[a]	n.d.[a]	n.d.[a]
Cr_2O_3	0.2	0.15	0.15	0.12	0.68	0.67	0.63	n.a.
FeO	12.2	10.7	10.7	n.d.[b]	n.d.[b]	n.d.[b]	n.d.[b]	n.d.[a]
FeO_T	n.d.[a]	n.a.	n.a.	14.15	18.60	17.86	18.11	10.53
MnO	0.36	0.24	0.24	0.13	0.41	0.38	0.41	0.16
MgO	10.5	8.31	8.32	8.21	9.49	9.57	9.19	10.46
CaO	5.98	6.04	6.05	5.79	8.19	8.09	7.77	10.57
Na_2O	2.66	4.15	4.16	4.13	2.80	2.72	2.70	2.18
K_2O	0.67	1.07	1.07	1.02	0.13	0.16	0.14	0.42
P_2O_5	0.96	1.39	1.39	1.47	0.57	0.61	0.62	0.26
F	n.d.[c]	n.d.[c]	n.d.[c]	n.d.[c]	n.d.[c]	0.56	0.55	n.d.[c]
SO_3	0.75	1.52	0.75	n.d.[c]	n.d.[c]	n.d.[c]	n.d.[c]	n.d.[c]
Cl	n.d.[c]	0.35	0.00	n.d.[c]	0.57	0.15	0.21	n.d.[c]
-O = F + Cl	n.d.[c]	n.d.[c]	n.d.[c]	n.d.[c]	0.07	0.27	0.28	n.d.[c]
Total	100.0	101.0	100.0	100.0	98.78	98.58	96.82	98.58
Mg#[d]	54	52	56	55	52	53	52	68
H_2O in synthetic glass (wt. %)			n.d.[c]	n.d.[c]	n.d.[c]	0.07[e]	1.67[e]	0.4[e]

* McSween et al (2006a).

~ Humphrey RAT1 composition from Gellert al. (2006).

¥ Synthetic composition from Nekvasil et al. (submitted).

ǂ Synthetic composition from McCubbin et al. (2008).

C Natural terrestrial olivine tholeiite composition as published in Whitaker et al. (2007a).

[a] All Fe measured as FeO

[b] All Fe reported as FeO_T

[c] Not analyzed.

[d] Mg# = Molar Mg/(Mg + Fe^{2+}) assuming an Fe^{2+}/Fe_{Tot} ratio of 0.85.

[e] Measured by FTIR (not included in total).

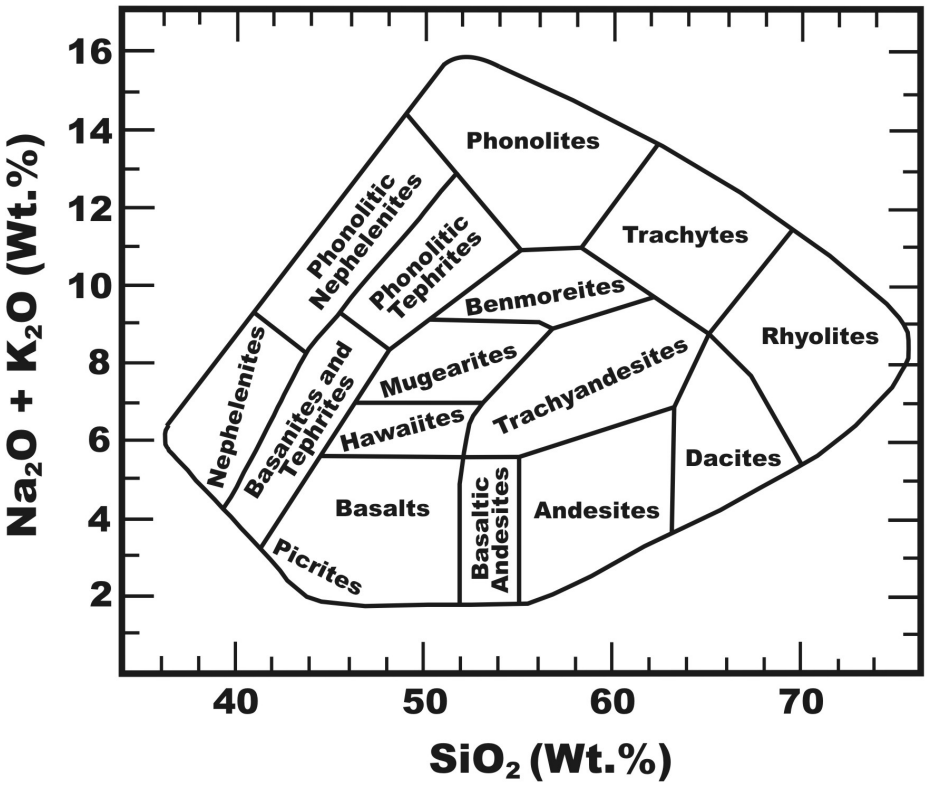

Figure 1.1. Volcanic rock classification diagram (Le Bas, 1964), signifying the range of compositions found in intra-continental hotspots or continental rifts on Earth based on silica and alkali content.

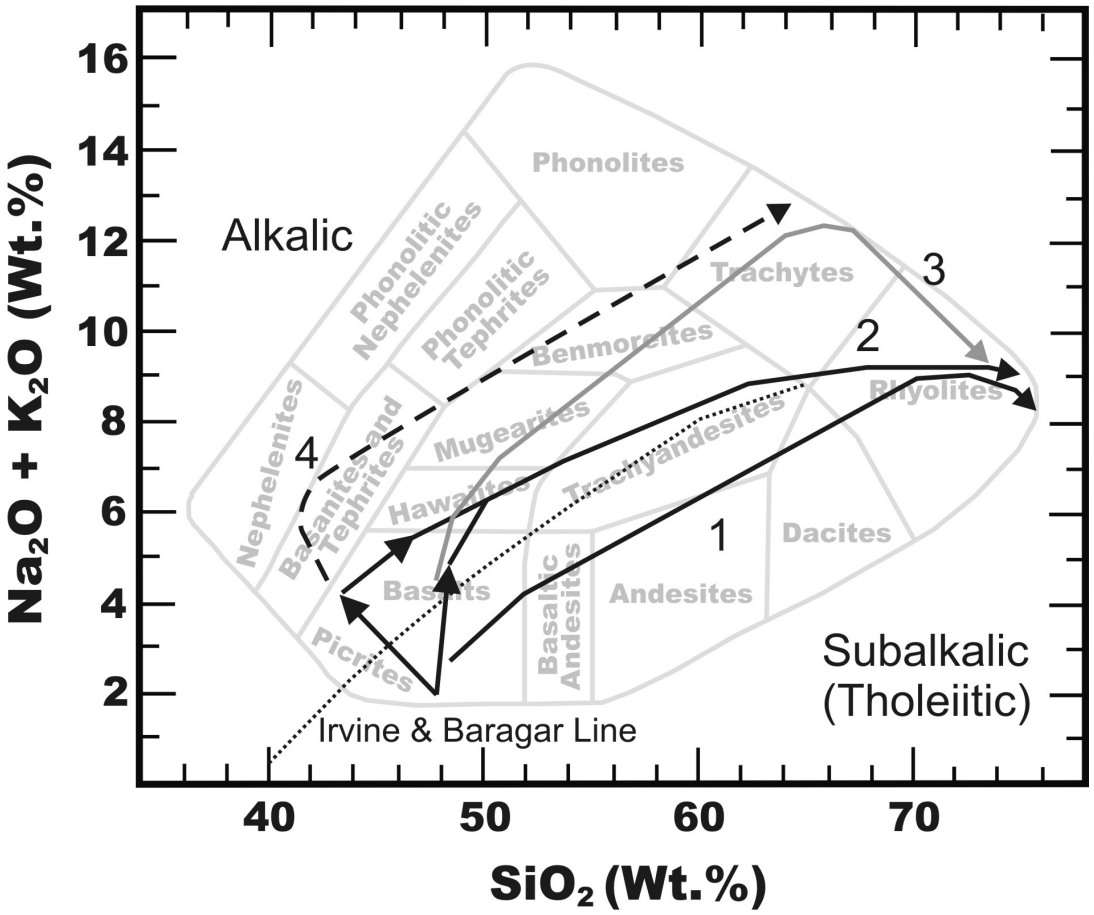

Figure 1.2. Volcanic rock classification diagram (Le Bas, 1964) overlaid with variation diagram portraying the three silica-saturated composition trends observed on Earth in intra-plate regions. (1) ocean island tholeiitic series; (2) potassic silica-saturated alkalic series; (3) sodic silica-saturated alkalic series; and (4) the primary silica-undersaturated alkalic series. The Irvine and Baragar line (adopted from Irvine and Baragar, 1971) separate the alkalic and subalkalic fields. Arrows point in the down-temperature direction.

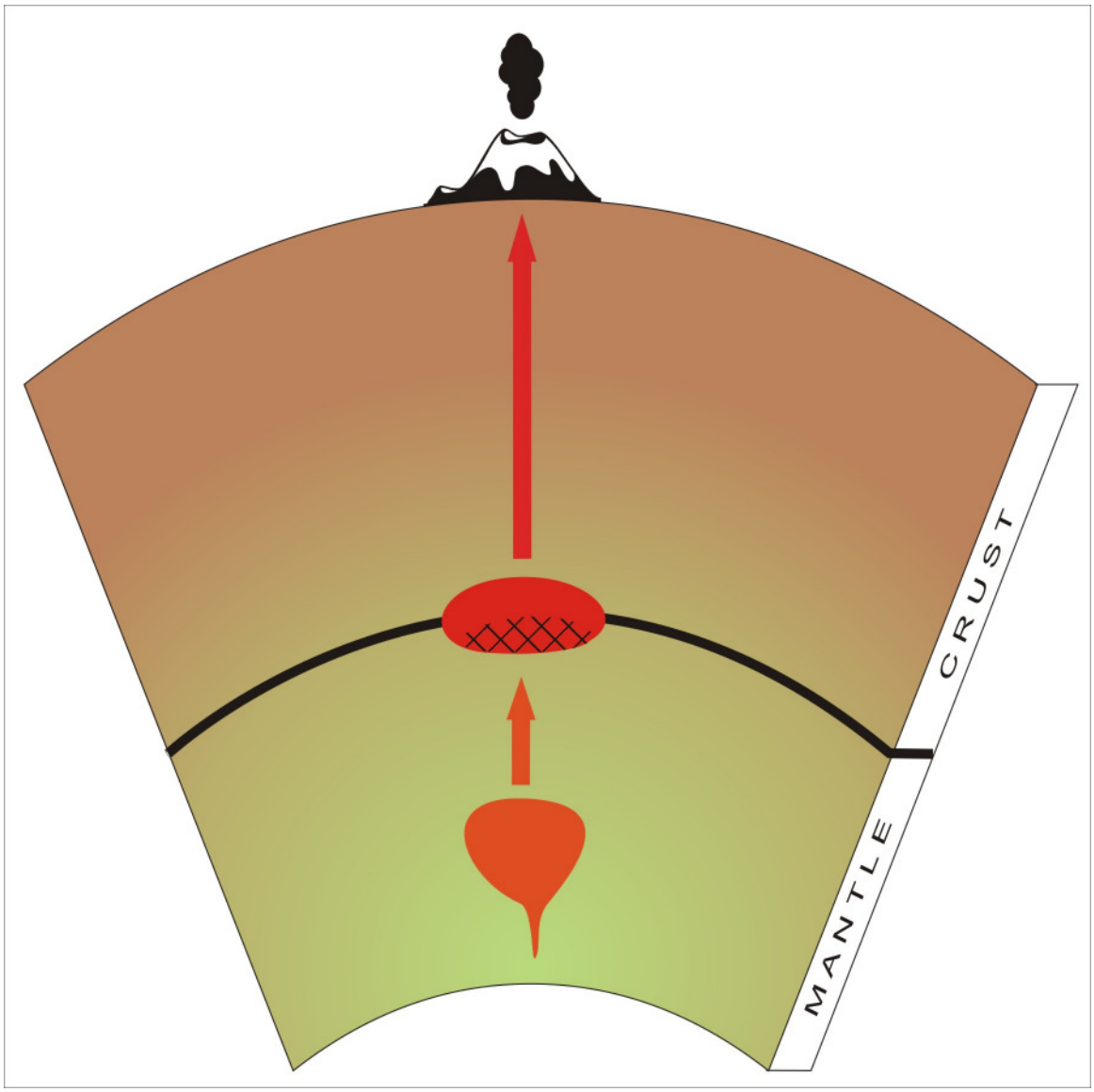

Figure 1.3. Schematic illustrating the process of single-stage fractional crystallization at the base of a thick crust in which liquids residual to fractionation ascend to the surface.

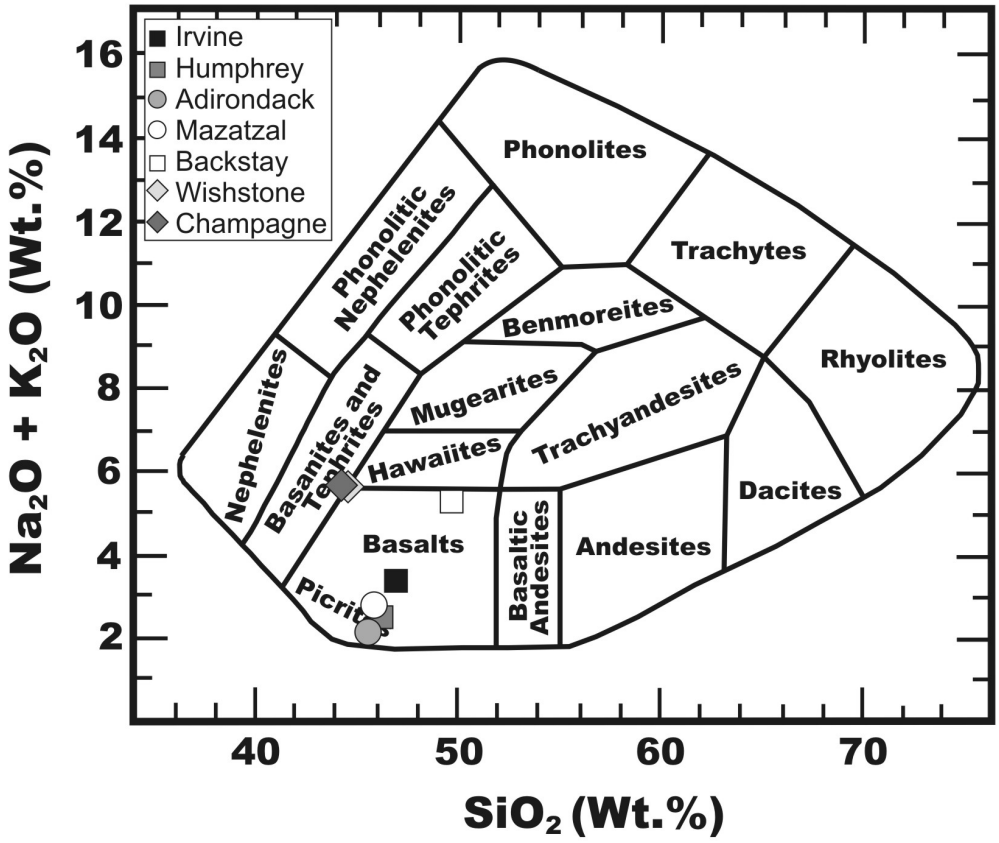

Figure 1.4. Total alkalis vs. silica of the martian surface rocks Irvine, Humphrey, Wishstone, Backstay, Champagne, Adirondack and Mazatzal found in Gusev Crater and analyzed by the MER Rover Spirit plotted on the volcanic rock classification diagram of Le Bas (1964).

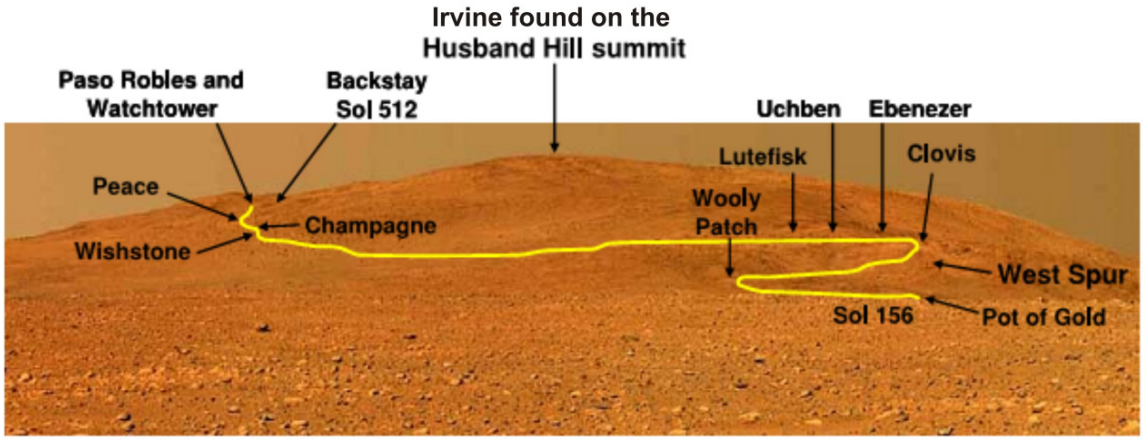

Figure 1.5. Image taken by the MER rover Spirit overlaid with its traverse up the Columbian Hills (Ming et al., 2006). The locations of different rocks analyzed are also shown.

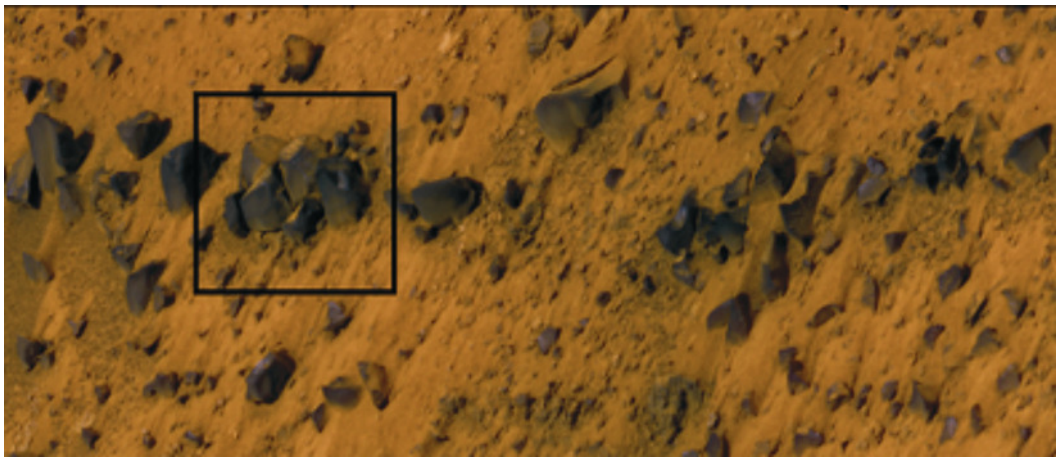

Figure 1.6. Irvine class rocks found in a linear pattern on the summit of Husband Hill. Image ~2m long; see Figure 1.7 for blown up section. (McSween et al., 2006a)

Figure 1.7. Irvine class rocks (image 25 cm across), also found on the summit of Husband Hill (McSween et al., 2006a).

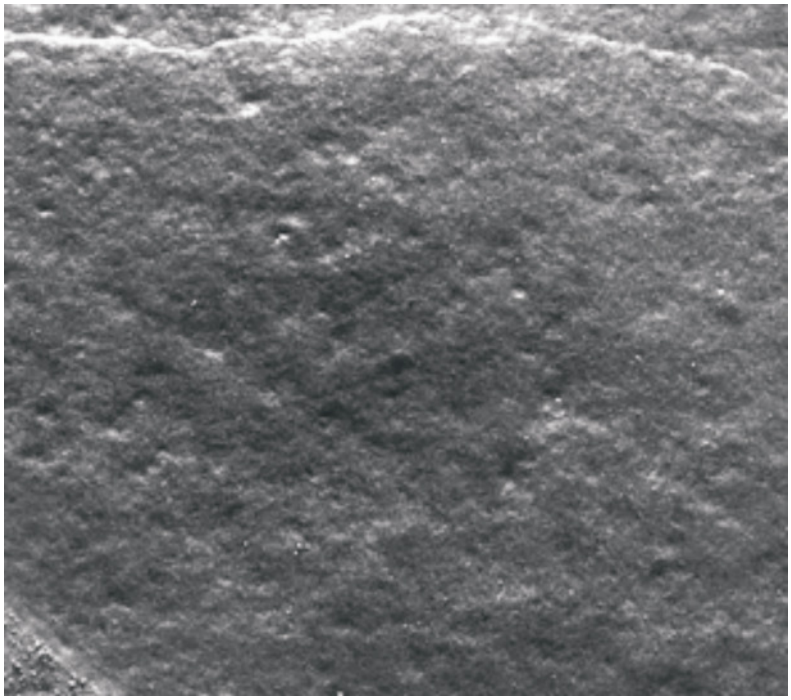

Figure 1.8. Radiometrically calibrated MI image of Irvine taken by MER Rover Spirit showing its fine grained texture (~16 mm high) (McSween et al., 2006a).

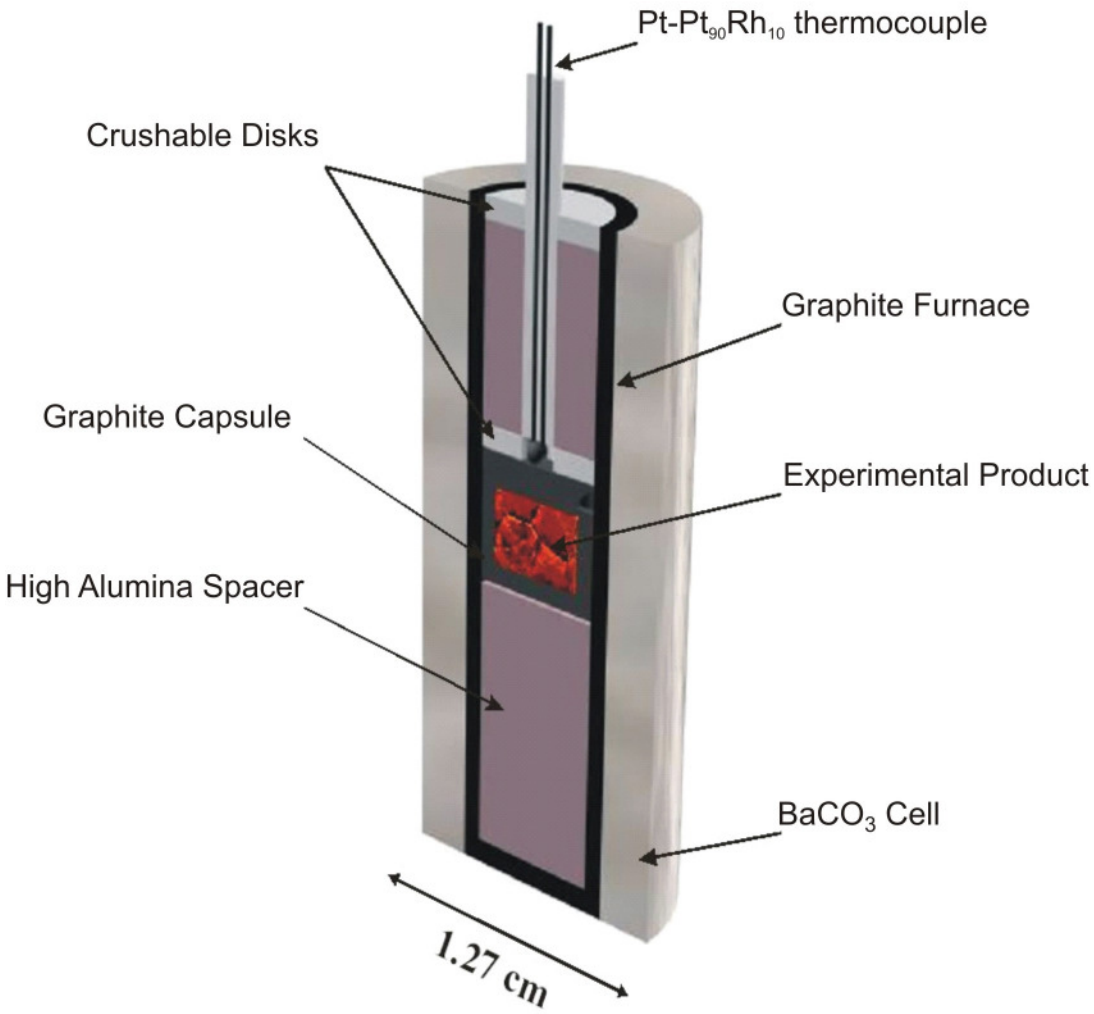

Figure 1.9. Schematic of the Ba-carbonate cell assembly used for the equilibrium crystallization experiments conducted in solid-media (piston-cylinder) pressure apparatus.

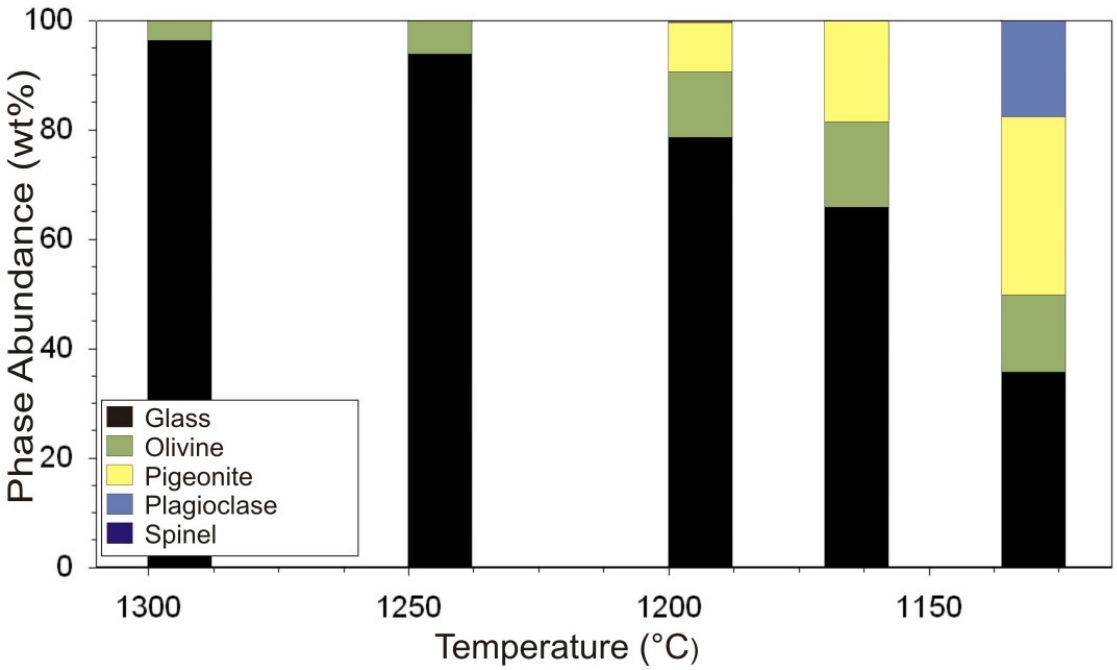

Figure 1.10. Calculated abundances of phases formed in crystallization experiments on Irvine composition liquid with 0.01 wt.% H_2O at 9.3 kbars. Abundances were calculated using the least squares mass balance routine of the IgPet software suite (Carr, 2002).

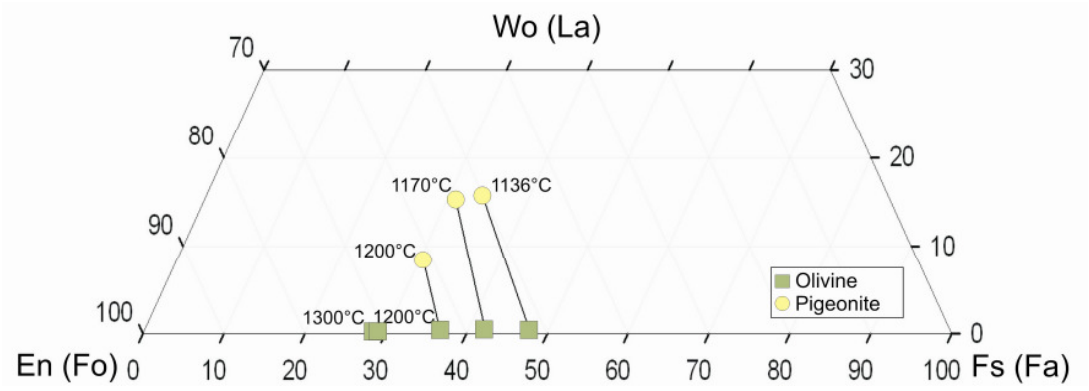

Figure 1.11. Projected compositions of ferromagnesian phases crystallized from experiments on Irvine with 0.01 wt.% H_2O at 9.3 kbars. Phases plotted using the projection scheme of the program QUILF (Andersen et al., 1993). Tielines connect phases co-existing at the indicated temperatures.

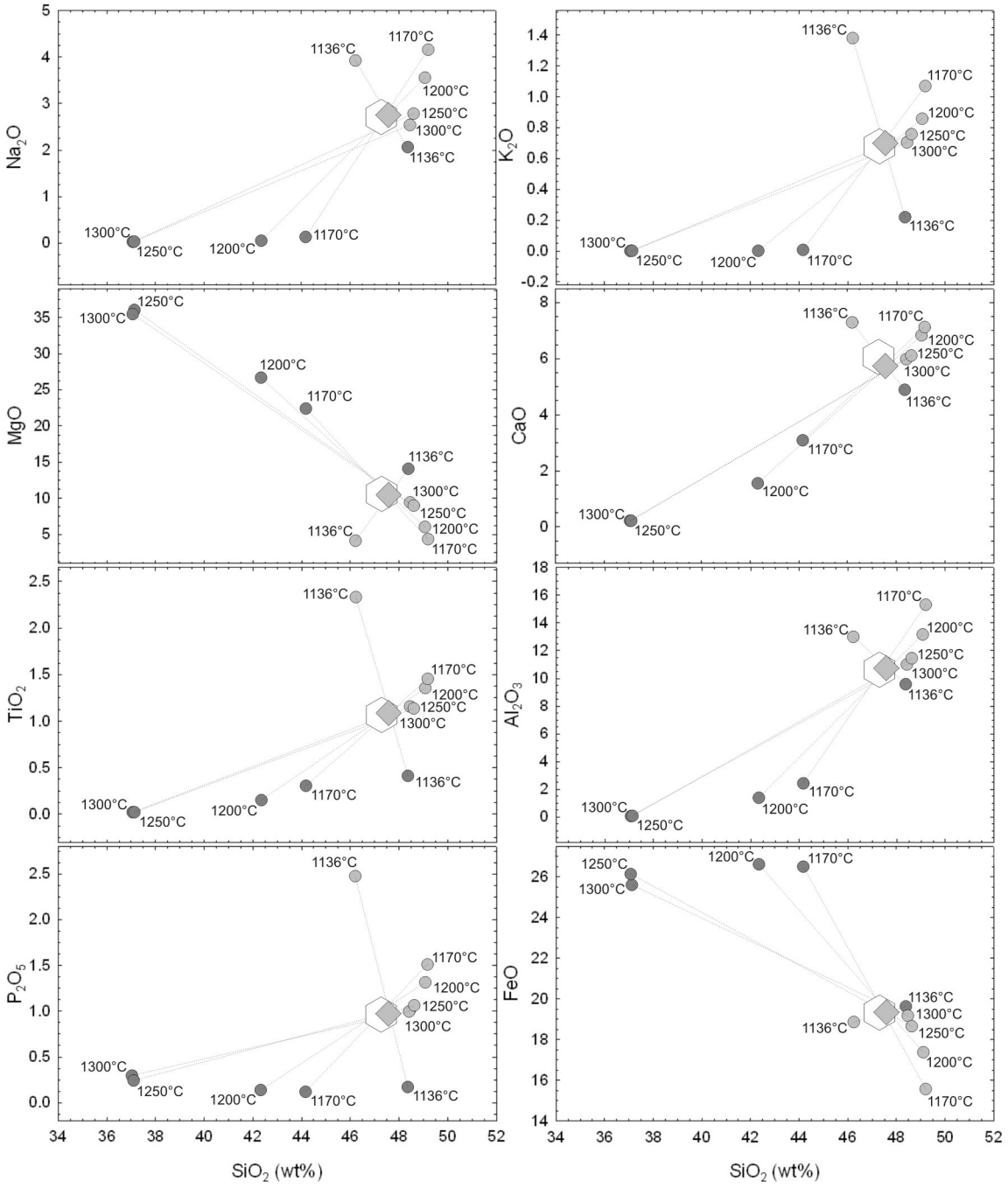

Figure 1.12. Harker-variation diagram for residual liquids (grey circles) and bulk solids (dark grey circles) from experiments on Irvine with 0.01 wt.% H_2O at 9.3 kbars. Irvine bulk rock composition analyzed by rover Spirit re-normalized after subtracting out volatiles (SO_3) (open hexagon) and IRVsynth Dry (grey diamonds) are also represented. Tielines connect residual liquid and solid phases co-existing at the indicated temperatures.

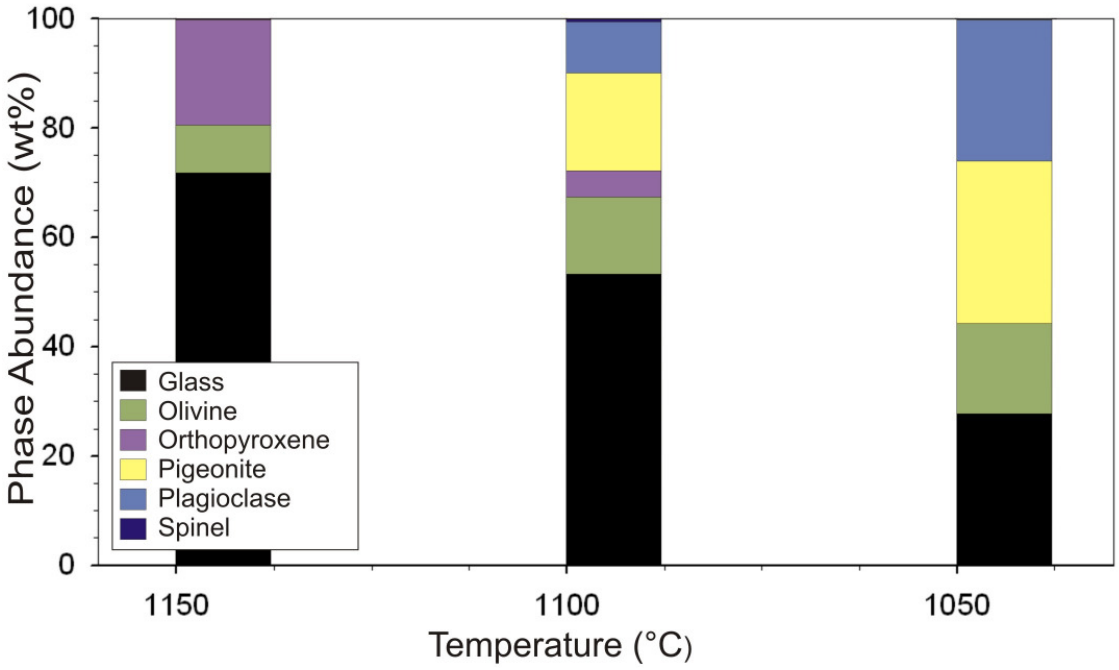

Figure 1.13. Calculated abundances of phases formed in crystallization experiments on Irvine composition liquid with 1.0 wt.% H_2O at 9.3 kbars. Abundances were calculated using the least squares mass balance routine of the IgPet software suite (Carr, 2002).

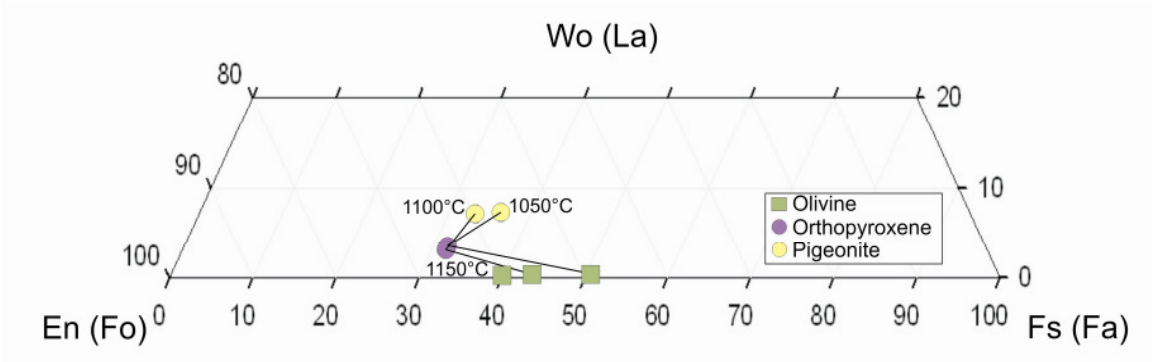

Figure 1.14. Projected compositions of ferromagnesian phases crystallized from experiments on Irvine with 1.0 wt.% H_2O at 9.3 kbars. Phases plotted using the projection scheme of the program QUILF (Andersen et al., 1993). Tielines connect phases co-existing at the indicated temperatures.

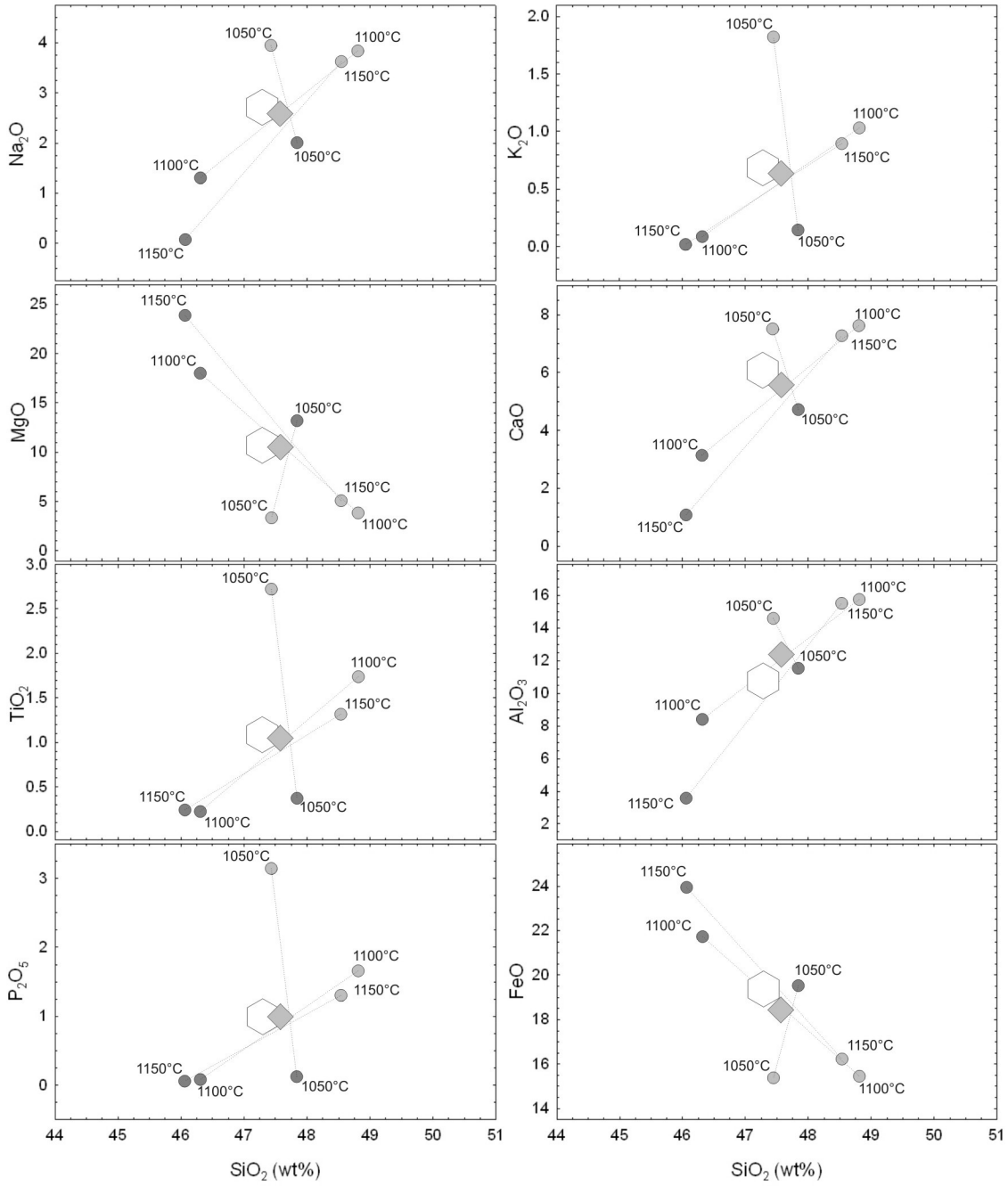

Figure 1.15. Harker-variation diagram for residual liquids (grey circles) and bulk solids (dark grey circles) from experiments on Irvine with 1.0 wt.% H_2O at 9.3 kbars. Irvine bulk rock composition analyzed by rover Spirit re-normalized after subtracting out volatiles (SO_3) (open hexagon) and IRVsynth Dry (grey diamonds) are also represented. Tielines connect residual liquid and solid phases co-existing at the indicated temperature.

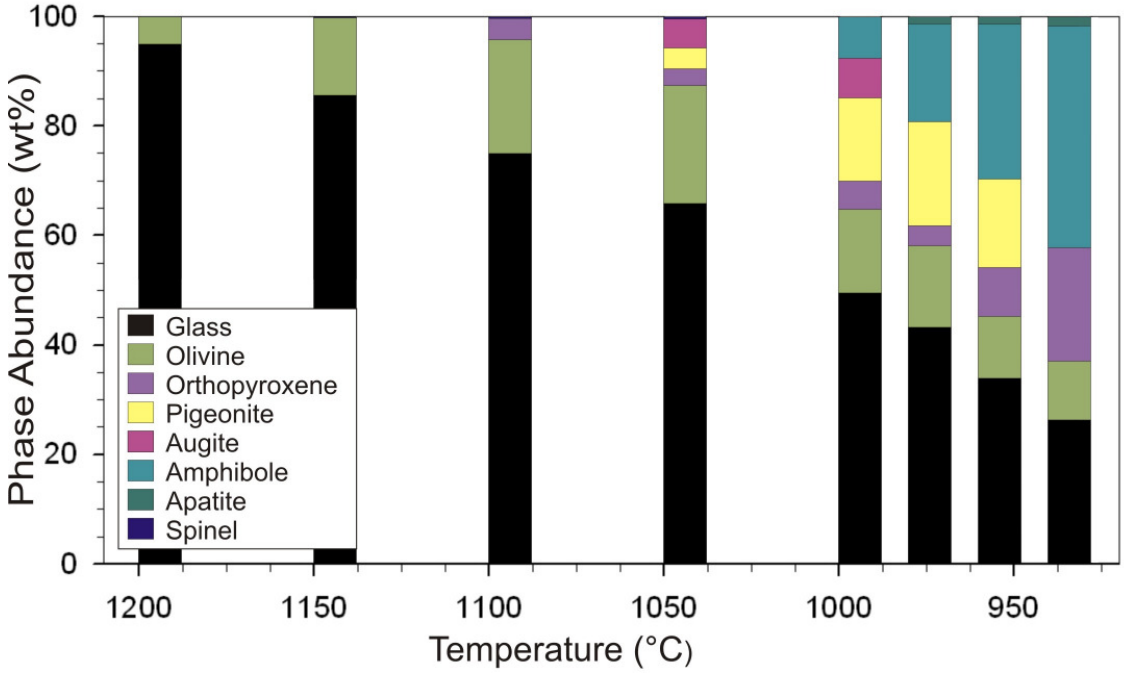

Figure 1.16. Calculated abundances of phases formed in crystallization experiments on Irvine composition liquid with 2.0 wt.% H_2O at 9.3 kbars. Abundances were calculated using the least squares mass balance routine of the IgPet software suite (Carr, 2002).

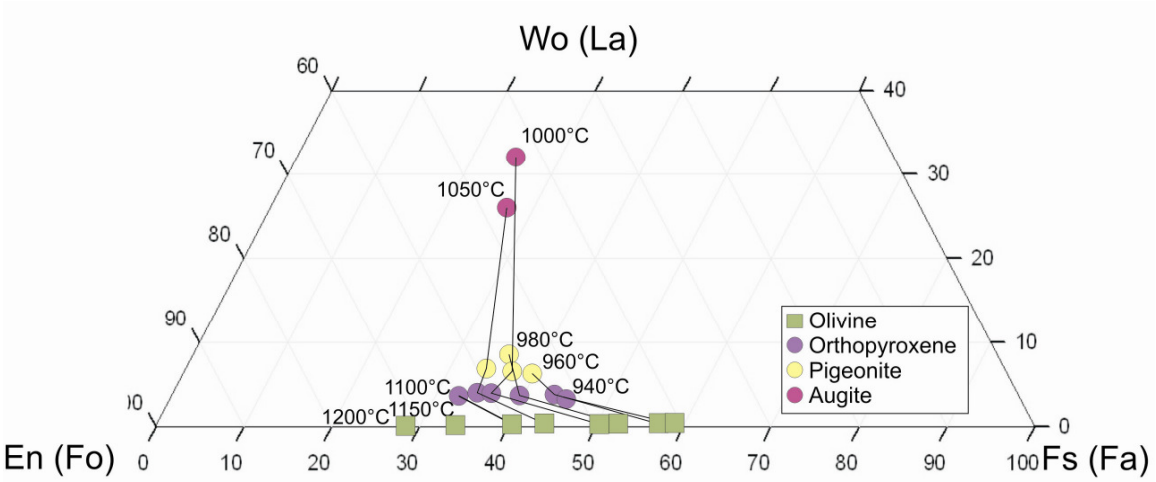

Figure 1.17. Projected compositions of ferromagnesian phases crystallized from experiments on Irvine with 2.0 wt.% H_2O at 9.3 kbars. Phases plotted using the projection scheme of the program QUILF (Andersen et al., 1993). Tielines connect phases co-existing at the indicated temperatures.

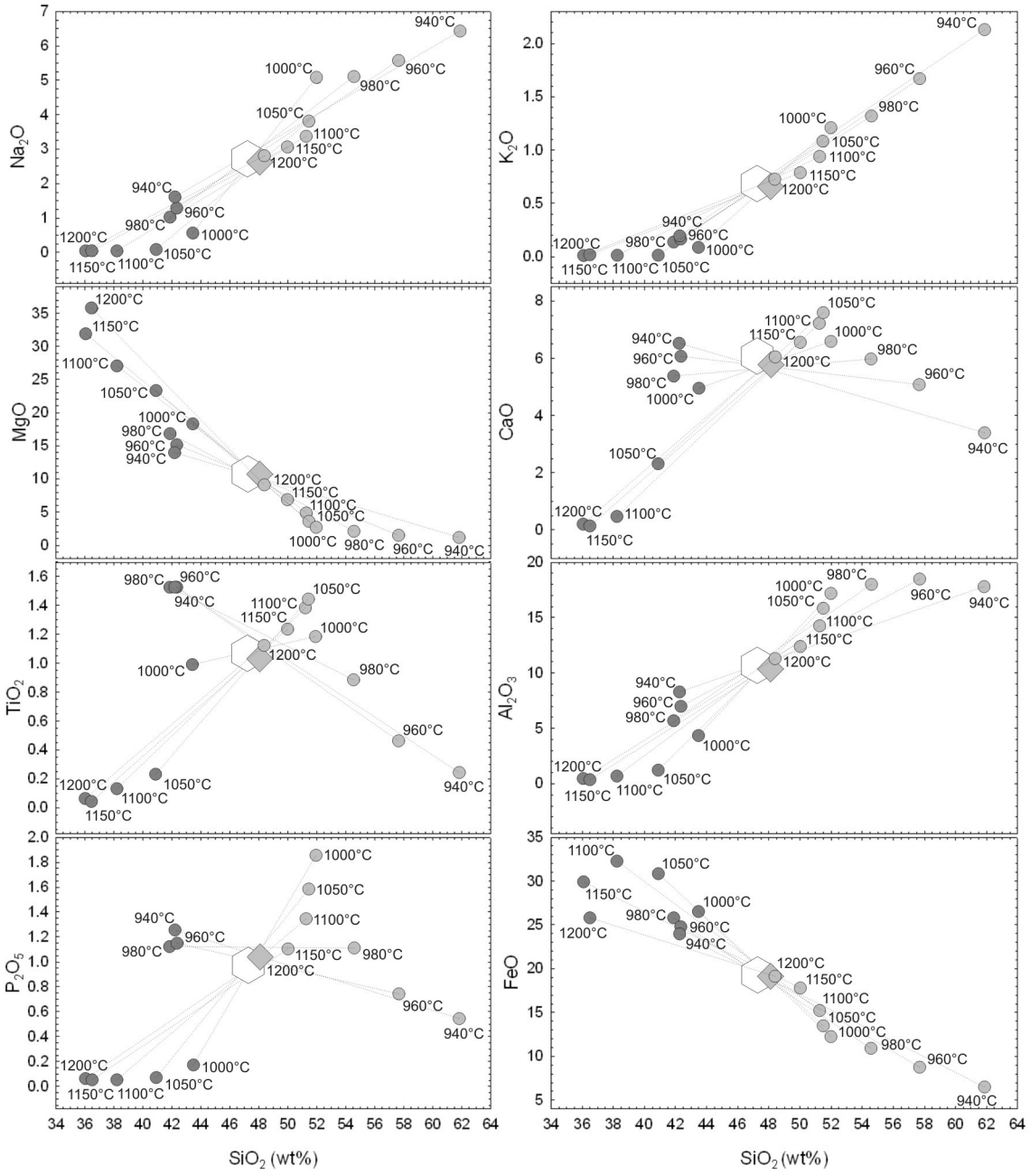

Figure 1.18. Harker-variation diagram for residual liquids (grey circles) and bulk solids (dark grey circles) from experiments on Irvine with 2.0 wt.% H_2O at 9.3 kbars. Irvine bulk rock composition analyzed by rover Spirit (open hexagons) and IRVsynth WetHi (grey diamonds) are also represented.

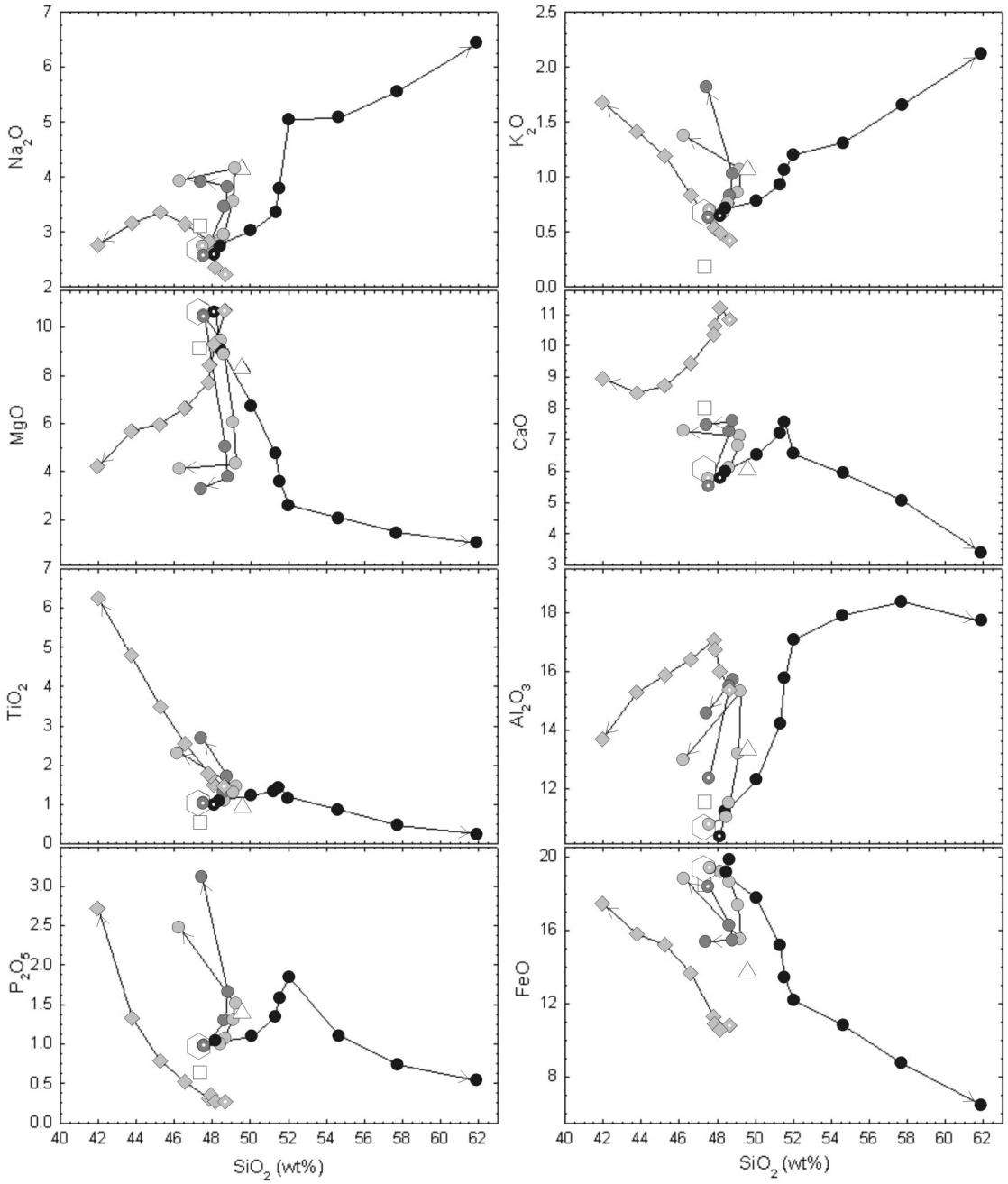

Figure 1.19. Harker-variation diagram for the residual liquids from experiments performed under "dry" (grey circles), "moderately wet" (dark grey circles) and "wet" (black circles) conditions with experimental compositions represented by white centered circles of corresponding color. For temperatures, see previous figures. Bulk rock compositions, as analyzed by rover Spirit, for Irvine (open hexagon), Humphrey (open square) and Backstay (open triangle) are also represented. Grey diamonds represent crystallization experiments (1280°C - 1160°C in increments of 20°C) performed on a terrestrial olivine tholieitte under anhydrous conditions at 9.3 kbars (Whitaker et al., 2007a).

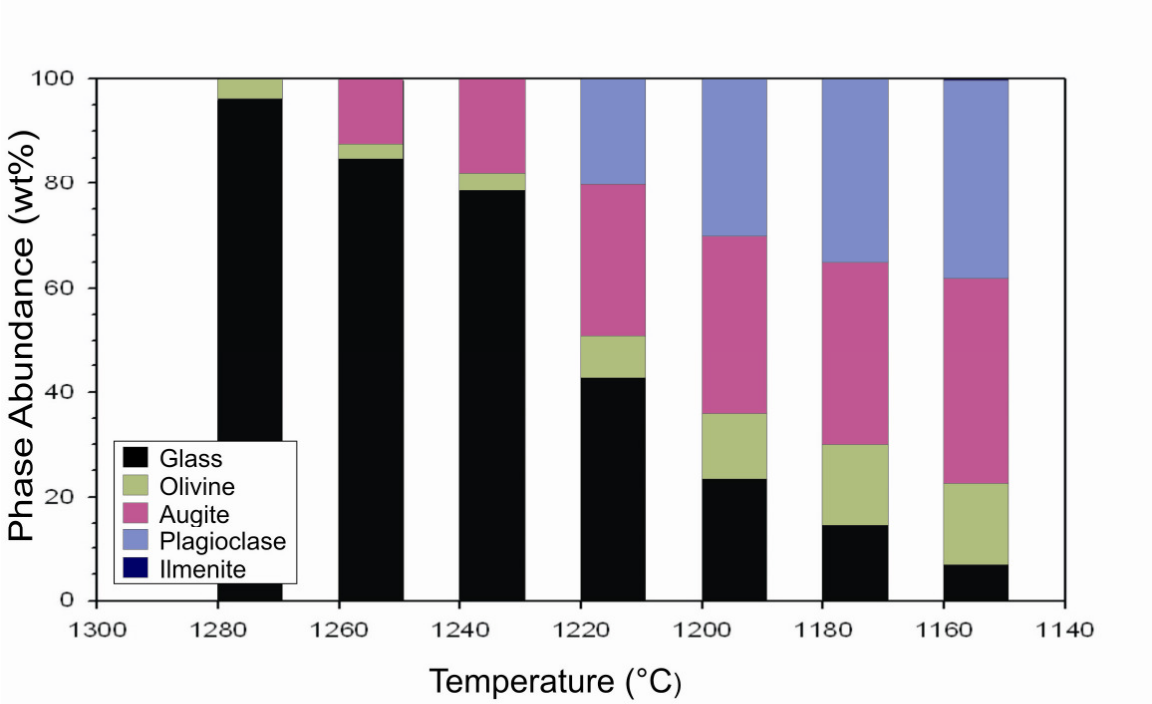

Figure 1.20. Calculated abundances of phases formed in crystallization experiments on "dry" ICPP123 260, a natural terrestrial olivine tholeiite from the Snake River Plain, with 0.05 bulk wt.% H_2O at 9.3 kbars(Whitaker et al., 2007a).

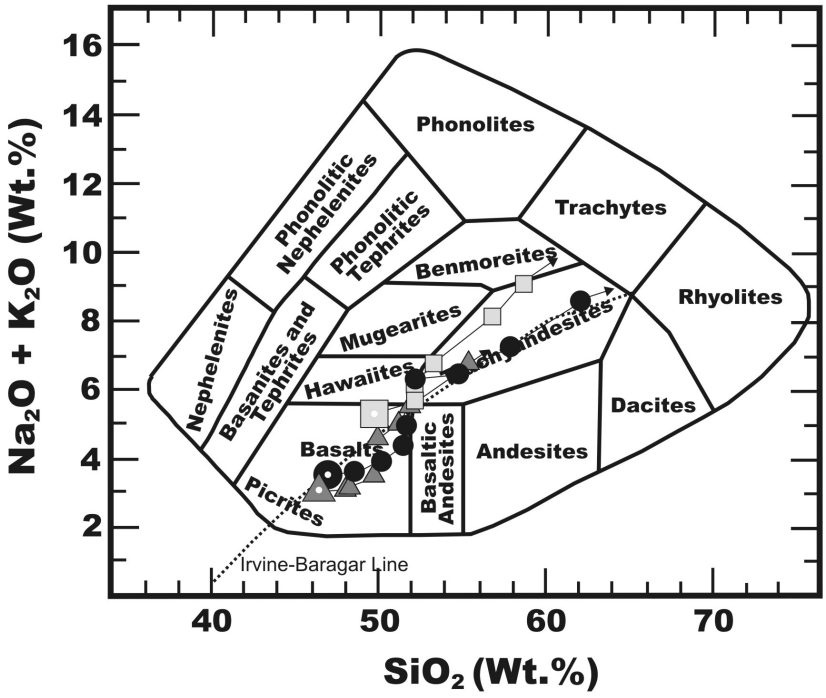

Figure 1.21. Volcanic rock classification diagram (Le Bas, 1964) signifying range of rock compositions produced along the silica enrichment trends of Irvine (black circles), Humphrey (grey squares) (McCubbin et al, 2008) and Backstay (dark grey triangles) (Nekvasil et al., submitted). Arrows indicate the down-temperature direction. Irvine-Baragar line (dotted) (Irvine and Baragar, 1971) separates the alkalic and subalkalic fields.

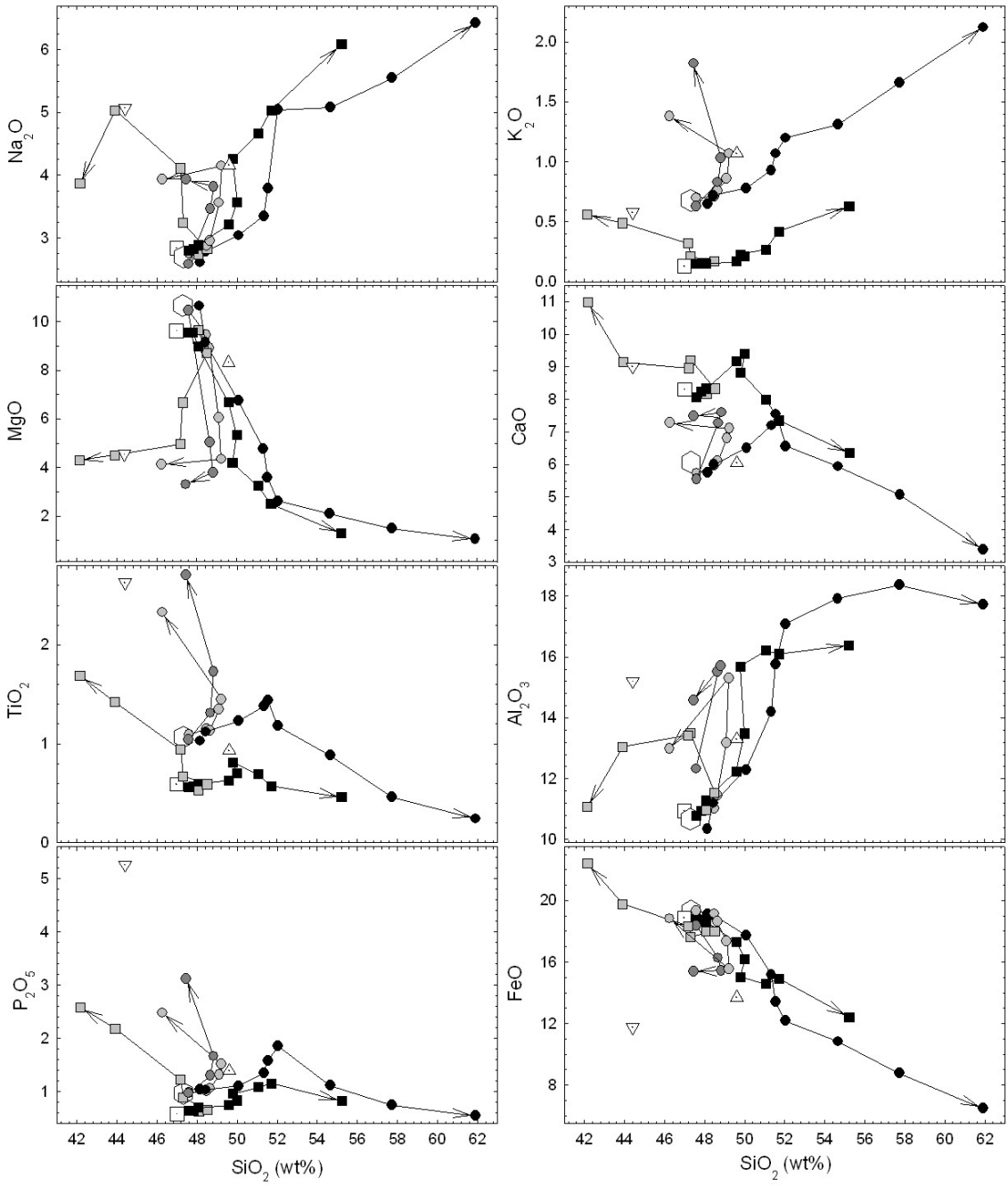

Figure 1.22. Comparison of liquid evolution of Irvine (circles with 0.01 wt.% water (grey), 1.0 wt.% water (dark grey) and 2.0 wt.% water (black)) and Humphrey (squares with 0.07 wt.% water (grey) and 1.67 wt.% water (black)) (McCubbin et al., 2008) in comparison to Wishstone composition (inverted open triangle). The compositions of Gusev Crater rocks Irvine (open hexagon), Humphrey (open square), and Backstay (open triangle) are also shown for comparison. Arrows indicate the down-temperature direction of liquid evolution.

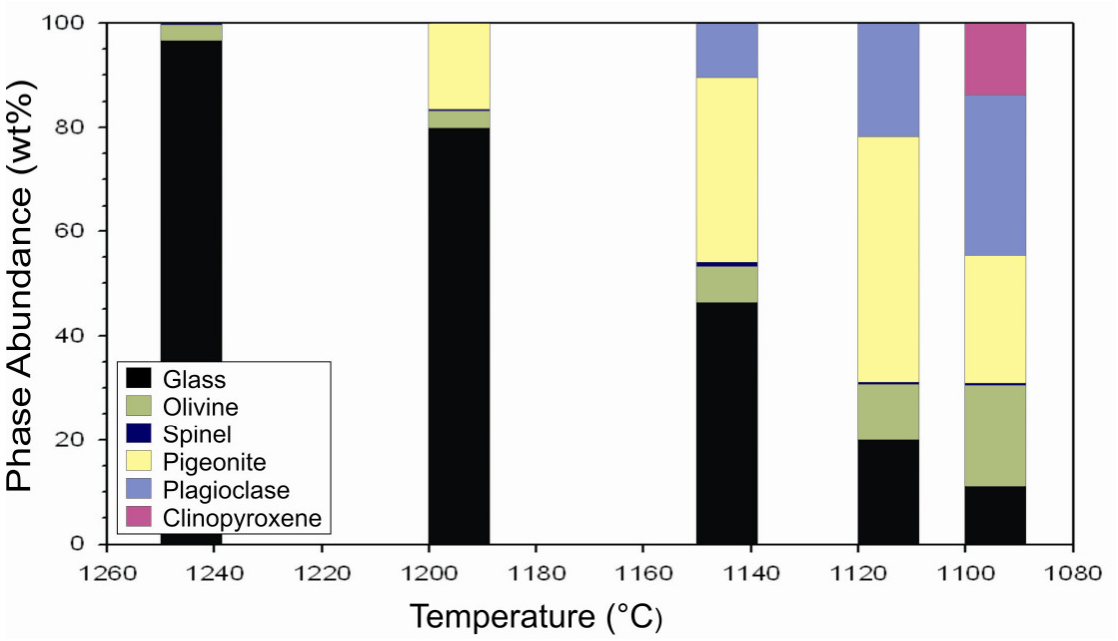

Figure 1.23. Calculated abundances of phases formed in crystallization experiments on Humphrey composition with 0.07 bulk wt.% H_2O at 9.3 kbars (McCubbin et al., 2008). Humphrey composition is a synthesized material derived from Humphrey bulk rock (HRAT1) a picritic martian basalt within the Gusev Crater (Gellert et al., 2006).

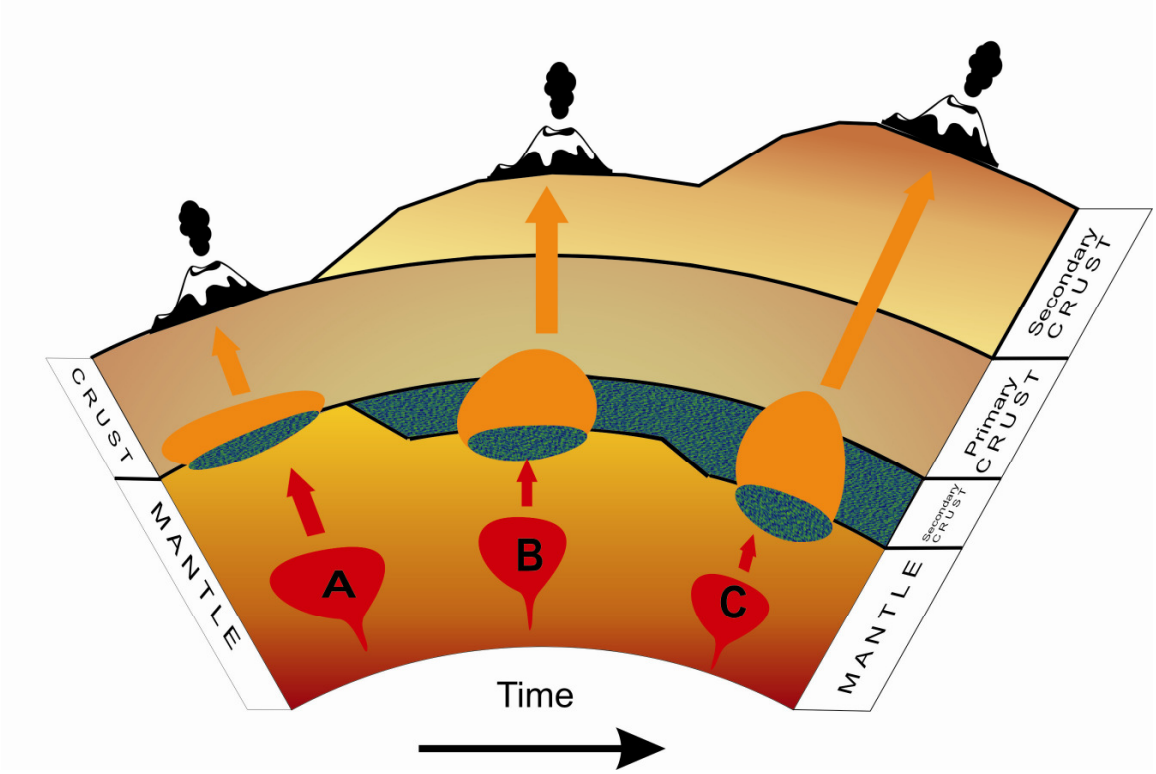

Figure 1.24. Schematic illustrating the evolution of martian crust over time given the presence of fractional crystallization; depicts both primary and early secondary crust being overlaid by later secondary crust.

Chapter 2

The effect of pressure on the phase equilibria of Irvine composition magmas

1. INTRODUCTION

Whitaker at al. (2007a) determined experimentally that "dry" tholeiitic magmas produce residual liquids with strong silica depletion if ponded at the base of a thick crust, but the extent of silica depletion decreases if ponded at shallower levels. This readily explains the range of magma types associated with anorthosites in areas of thick continental crust and the silica-enrichment trend of the tholeiitic ocean island suites. Although there is no indication that the martian crust is anywhere as thin as in the Earth's oceans, the range of thicknesses proposed by Norman (2002) and Taylor et al. (2006) suggest the importance of assessing Irvine phase equilibria not only at ~70km depth, but also for the case of ponding at shallow-mid crustal levels or possibly at the base of a thinner crust (Figure 1.24 and 2.1). The experiments described below investigate the nature of the crystallizing assemblages and residual liquids at 2.8 kbars (~23 km depth) in comparison with the crystallizing assemblages observed a greater depth and pressure in Chapter 1. This new depth represents an area of shallow-mid crustal ponding or is possibly reflective of the crustal thickness early in martian history just after formation of the primary crust.

2. EXPERIMENTAL/ANALYTICAL PROCEDURE

2.1 Strategy

Crystallization experiments were conducted on Irvine composition in graphite capsules. This crystallization study relates the nominally anhydrous experiments performed at 9.3 kbars (~70 km in depth) in Chapter 1 with additional nominally anhydrous crystallization experiments performed at 2.8 kbars (~23 km depth). After the run products were analyzed optically and by EPMA, the abundance of each phase, residual liquid and crystalline material, were computed by mass balance.

2.2 Experimental Procedure

2.2.1 *Starting Materials*

The powder mix for this pressure study was created based on the Irvine data first published by McSween et al. (2006a), which was acquired by analyses performed by the APXS spectrometer on the MER Rover Spirit (Table 2.1). The starting material was created by mixing oxides and Fe^0 powders sequentially by volume, starting with smaller oxide components and eventually adding in those oxides comprising larger proportions, in an automatic agate mortar/pestle grinder for 3.5 hours. The $Fe^{3+}/\Sigma Fe$ value of the mixture was 0.16. The composition of this synthetic Irvine mixture IRVsynth (IRV006mr) is reported in Table 2.1.

2.2.2. *Piston-Cylinder Experiments*

Experimental Set-up

All experiments were on "dry" material. As described in Chapter 1, this was obtained by first loading the sample, IRVsynth, into a graphite capsule, then placing the loaded capsule into a silica glass tube in the presence of a Fe^0 oxygen "getter" with a glass spacer for the purpose of separation and then drying the sample and capsule at 800°C under vacuum for 20 minutes in a vertical tube furnace. After cooling rapidly with a cold water bath, the capsule was then loaded into a cell assembly (same as that described in Whitaker et al., 2007a), placed into a ½ inch piston cylinder (piston out method) and pressurized. The time between rapidly cooling and pressurization was kept to a minimum in order to avoid H_2O (re)absorption. Once pressurized, the temperature was raised to a melting temperature of 1372°C, a value above the liquidus, and allowed to melt for 2.5 hours in order to homogenize the resulting liquid. After this time, the sample was rapidly dropped isobarically to the chosen crystallization temperature and allowed to crystallize for no less than 2.5 days. The temperature was controlled by a Pt-Pt_{90}-Rh_{10} thermocouple, and the run was quenched isobarically. The water content was verified to be 0.01 wt.% by micro-FTIR.

Since two different martian crustal depths were being investigated, the pressure the experimental runs were kept at varied. In order to simulate pressures at the crust-mantle boundary of Mars (~70 km deep) the piston-cylinder experiments were performed at 9.3 kbars (10 kbars nominal), while a lower pressure of 2.8 kbars (3.5 kbars nominal) was selected to simulate pressures at shallow-mid crustal depth (~23 km deep).

Oxygen Fugacity

Finally, in order to prevent oxygen fugacity from increasing beyond the graphite-CO-CO_2 (GCO) buffer, a graphite capsule was used, though this only provides an upper fO_2 limit (Eugster and Skippen, 1967). This technique yields values between 1.0 and 2.5 log units below the fayalite-magnetite-quartz (FMQ) at the pressure of 9.3 kbars (Whitaker et al., 2007a). However, at lower pressure the GCO buffer is quite reducing and at 1 bar yields an oxygen fugacity below iron-wustite (French and Eugster, 1965).

2.3 Analytical Procedure

2.3.1 *EPMA Analysis*

After each experiment, a thin section of the run products was made and examined first optically and then, after carbon coating analyzed by electron microprobe. Electron probe microanalysis (EPMA) was performed at Stony Brook University using a Cameca Camebax electron microprobe (EMP), equipped with four wavelength dispersive spectrometers. For the analyses, an accelerating voltage of 15 kV and a nominal beam current of 10nA were used. However, due to the volatility of sodium, for Na-bearing phases the largest possible raster size was used and a time-zero correction was emplaced in order to minimize unknown analytical problems that occur during highly focused electron beam analysis on such matrices. The correction technique of Nekvasil et al. (2004) was also adopted for sodium loss, as a means to verify the aforementioned steps success or if needed correct for the sodium loss. The technique is comprised of adding sodium back to the analysis until there is no normative corundum present in the norm of a Na-bearing phase. The next step in the data processing was to perform mass-balance

calculations using the IgPet Program Suite (Carr, 2002) by means of a least squares routine. These calculations were used not only to ensure that the analyses were reasonable and that no phase was overlooked during microprobe analysis, but also to quantitatively assess the abundance of each phase present. The calculated mineral abundances were then used to determine the total residual solids present at each crystallization temperature.

2.3.2. *Micro-FTIR Spectroscopy*

In order to determine the water content of both the hydrous glasses and of the melting and crystallization runs, infrared spectroscopic measurement were conducted on the experimental glass products. These analyses were conducted at room temperature in transmittance mode with a Thermo Nicolet 20SXB FTIR spectrometer. The IR spectra were collected from doubly polished wafers of the run products over the mid-IR (1400-4000 cm^{-1}) to near-IR regions (3700-6500 cm^{-1}) using a KBr beam splitter, MCT/A detector, and globar source. Before data collection, both the spectrometer and the IR objective were purged with dry nitrogen gas at a rate of 15 1/min. The water content was measured in total dissolved water concentrations and was determined for each glass from the intensity of the broad band at 3570 cm^{-1} following the calculation scheme of Mandeville et al. (2002). Approximately 1024 scans were performed for each IR spectrum acquired at a resolution of 4 cm^{-1}. Before each analysis, the point at which the beam would be focused was viewed optically to ensure that the FTIR beam passed only through glass.

3. RESULTS

The high pressure crystallization experiments that were kept at 9.3 kbars are the same as those discussed in Chapter 1 run under "dry" conditions, and should be referenced accordingly. Low pressure crystallization experiments were kept at 2.8 kbars throughout the entire sequence of melting, crystallization and quench. The temperature range for these experiments was from 1150-1100°C with the starting water content of 0.01 wt.% water.

3.1. *Mineral Phases*

Table 2.2a lists the mineral phases and their respective compositions for each experimental temperature crystallizing at 2.8 kbars; the abundance of each phase is given in Table 2.3. At the crystallization temperature of 1150°C, olivine and Cr-spinel were present in the assemblage. The olivine is slightly more forsteritic than that at 9.3 kbars(interpolated between temperatures close to 1150°C at 9.3 kbar). At 2.8 kbar, olivine is the only silicate to form. At 9.3 kbar, pigeonite has already crystallized in significant abundance by this temperature.

Below 1150°C, a new phase appears. This phase consists of rounded balls of metallic iron that contain variable amounts of phosphorus (Table 2.2a), with the metallic iron containing between 5.6 – 12.5 wt.% P_2O_5 at 1125°C and ~0.2 wt.% P_2O_5 at 1100°C. They are found throughout the sample, but are concentrated around the graphite capsule. Given that these iron droplets comprise a significant amount of the run product and therefore affect mass balance they were included in the computed assemblage of Table 2.3. With the increased abundance of the iron balls, comes an increase in forsterite

content of the co-existing olivine. The compositional evolution of the bulk solids is represented in Table 2.4 and Figure 2.2.

3.2. *Liquid Evolution*

The liquidus temperature for the crystallization experiments of Irvine performed under low pressure conditions (2.8 kbars) lies between 1150°C and 1250°C; the solidus temperature is below 1100°C. Table 2.2b and Figure 2.2 shows the compositional evolution of the liquids residual to crystallization. These liquids show a clear silica-enrichment trend at this pressure.

However, due to the presence of the iron balls the liquid evolution is not valid due to the fact that instead of representing a viable run product, it represents an incompatibility within the experimental technique.

4. DISCUSSION

The liquid at 1150°C for the 2.8 kbar experiment, which did not have any Fe-balls, is more silica-rich than any of the reasonable liquid compositions produced at 9.3 kbars(Table 2.2b vs. Table 1.5b, respectively). This is caused by more extensive olivine crystallization at the lower pressure, which extends the early olivine fractionation line at high pressure to higher silica contents at the lower pressure (Figures 1.19 vs 2.2).

Below this temperature, olivine continues to be the dominant phase and only silicate through 1100°C for the low pressure experiments. This, in conjunction with the iron droplets, induces further silica enrichment. Although DiFrancesco et al. (2003) and Whitaker et al. (2008) determined that for a terrestrial tholeiite, low pressures enhance

extensive olivine stability at the expense of pyroxene, the presence of the iron balls may have affected phase equilibria in these experiments on Irvine. The iron balls appear to have formed from the melt by reduction of Fe^{2+} through reaction with graphite according to the overall reaction: $2FeO + C = 2Fe + CO_2$. This is a result of the low fO_2 imposed by the graphite at this pressure. As iron is removed from the melt by this process, the Mg# of the melt increases; this is reflected in the increase in Mg# of olivine with dropping temperature (Table 2.2a). Furthermore, this loss of iron will continuously change the bulk composition towards higher MgO/FeO ratios, while increasing the abundance of components not incorporated into olivine. This can change the temperature of appearance of additional silicates and their compositions, driving the residual liquids to different compositions than if the bulk composition were to remain constant.

In experiments performed by Whitaker et al. (2007a) on a terrestrial tholeiite under the same experimental conditions, the Fe^{2+} reduction problem was not evident. This tholeiite had a much lower Fe-content (and higher in alumina and calcia). It is thought that the higher Fe-content of Irvine may be the reason for this problem, occurring for Irvine experiments but not those on terrestrial olivine tholeiite. Therefore, the high Fe-contents of many martian rocks, including Humphrey, may have this same problem for all low pressure experiments conducted using graphite capsules.

Whitaker et al. (2007b) showed that there was no difference between the graphite and Fe-Pt capsules in crystallizing FTP rocks at high pressures with a terrestrial tholeiite. Since no difference between Fe-Pt capsules and graphite capsules was observed, perhaps Fe-Pt capsules should be used for all low pressure, high-Fe compositions since the Fe-soaked platinum capsules will not have much of an effect on the oxygen fugacity. For this

reason it is suggested that any future low pressure experiments on high-Fe compositions should be done in Fe soaked Pt capsules to verify if successful low-pressure experiments on martian type compositions (i.e. high-Fe) are possible.

4.1. The effect of pressure

Although the low pressure "dry" experiments are not useable once the Fe balls formed, the results for 1150°C indicate that, as seen for terrestrial tholeiite, low pressure will increase olivine crystallization at the expense of pyroxene. This will cause strong silica enrichment in residual liquids. Although wet experiments were not conducted, it is reasonable to expect that at low pressure silica-enrichment will also be produced from hydrous (2.0 wt.% H_2O) Irvine magmas as it was at high pressure. At very low pressure, the solubility of water is so low that there should be no difference between "wet" and "dry" Irvine liquids and both will likely show silica enrichment because of the dominance of olivine, just as is seen in terrestrial olivine tholeiite crystallized at 1 bar (DiFrancesco et al., 2003; Whitaker et al., 2007a). For this reason, it is likely that if Irvine-like basalts were produced by partial melting of the martian mantle early, while the crust was still relatively thin, the surface lavas would range from basalt to dacite and rhyolite, and olivine would be added to the lower crust. Only as the crust thickened and extensive magmatism caused source region dehydration would evolved low silica basaltic lavas dominate the surface.

Table 2.1. Composition of Irvine-class rocks and synthesized Irvine composition. Irvine Unbrushed and Irvine are the compositions analyzed by the APXS unit on-board the MER Spirit before and after SO_3 adjustment, respectively. IRVsynth is the composition of the synthetic mixture used in the experiments (as determined by Electron Probe Microanalysis of glass).

Oxide	Unbrushed Irvine*	Irvine*	IRVsynth ǂ
SiO_2	47.0	46.6	47.59
TiO_2	1.06	1.05	1.09
Al_2O_3	10.6	10.5	10.76
Fe_2O_3	7.68	7.61	n.d.[a]
Cr_2O_3	0.2	0.2	0.22
FeO	12.3	12.2	n.d.[b]
FeO_T	n.d.[c]	n.d.[c]	19.32
MnO	0.36	0.36	0.37
MgO	10.6	10.5	10.47
CaO	6.03	5.98	5.74
Na_2O	2.68	2.66	2.76
K_2O	0.68	0.67	0.70
P_2O_5	0.97	0.96	0.98
SO_3	2.37	0.75	n.d.[c]
Cl	0.45	0.00	n.d.[c]
Total	103.0	100.0	100.00
Mg#[d]	54	54	54
H_2O in synthetic glass (wt. %)			0.01[e]

* McSween et al (2006a)

ǂ Synthetic composition used for this study

[a] All Fe measured as FeO

[b] All Fe reported as FeO_T

[c] Not analyzed

[d] Mg# = Molar Mg/(Mg + Fe^{2+}) assuming an Fe^{2+}/Fe_{Tot} ratio of 0.85.

[e] Measured by FTIR (not included in total).

Table 2.2a. Compositions of co-existing minerals as a function of temperature for IRVsynth (0.01 wt.% bulk water[a]) at 2.8 kbars.

Phase	**Cr-Spinel**	**Olivine**			**High P Fe-metal Balls**	**Fe-Metal Balls**	**Low P Fe-Metal Balls**
Experiment	IRV018dr	IRV018dr	IRV019dr	IRV020dr	IRV019dr	IRV019dr	IRV020dr
Temperature (°C)	1150	1150	1125	1100	1125	1125	1000
SiO_2	0.77	35.95	36.32	36.39	0.09	0.10	0.04
TiO_2	2.41	0.05	0.07	0.06	0.06	0.09	0.03
Al_2O_3	16.31	0.04	0.05	0.06	0.01	0.00	0.00
Cr_2O_3	40.96	0.14	0.23	0.18	0.06	0.03	0.00
FeO	29.30	32.94	31.26	29.30	119.40	123.98	130.22
MnO	6.33	0.58	0.65	0.56	0.00	0.06	0.04
MgO	0.32	30.03	31.01	32.88	0.02	0.00	0.01
CaO	0.26	0.31	0.40	0.41	0.10	0.17	0.02
Na_2O	0.03	0.08	0.01	0.00	0.00	0.07	0.00
K_2O	0.34	0.02	0.00	0.01	0.02	0.03	0.01
P_2O_5	0.06	0.10	0.10	0.12	12.47	5.60	0.23
Total	97.10	100.23	100.09	99.95	132.22	130.12	130.60
Phase Comp. (mol %)	$Ul_6Mt_5Hy_{33}Cr_{55}$	$Fo_{62}(La_{0.38})$	$Fo_{64}(La_{0.59})$	$Fo_{66}(La_{0.59})$	n.a.	n.a.	n.a.

[a] measured by FTIR.

Table 2.2b. Compositions of glass as a function of temperature for IRVsynth (0.01 wt.% bulk water[a]) at 2.8 kbars.

Experiment (No.)	IRV018dr	IRV019dr	IRV020dr
Temperature (°C)	1150	1125	1100
SiO_2	49.77	53.68	53.99
TiO_2	1.24	1.38	1.37
Al_2O_3	13.40	14.61	14.61
Cr_2O_3	0.09	0.08	0.11
FeO	15.75	11.15	10.38
MnO	0.35	0.29	0.31
MgO	5.00	4.29	3.83
CaO	6.98	7.42	8.13
Na_2O	3.41	3.60	3.89
K_2O	0.77	0.87	0.87
P_2O_5	1.11	1.03	1.38
Total	97.88	98.41	98.86
Mg#[b]	40	45	44

[a] measured by FTIR.

[b] Mg# = Molar Mg/(Mg + Fe^{2+}) assuming an Fe^{2+}/Fe_{Tot} ratio of 0.85.

Table 2.3. Computed phase abundances at each experimental crystallization temperature for IRVsynth (0.01 wt.% bulk water) at 2.8 kbars. Sum of the squares of the residuals (s.s.r.) are presented for each computed assemblage.

Experiment (No.)	IRV018dr	IRV019dr	IRV020dr
Temperature (°C)	1150	1125	1100
Mode (wt.%)	Gl 79.1 Ol 20.8 Sp 0.1	Gl 72.5 Ol 23.5 Hi P Fe-Ball 0.8 Mod P Fe-Ball 3.2	Gl 71.5 Ol 23.5 Lo P Fe-Ball 5.0
Crystallinity (wt.%)	21	27.5	28.5
S.S.R.	0.134	0.098	0.098
H_2O in Glass (wt.%)	0.01 [a]	0.01 [a]	0.01 [c]

[a] measured by FTIR.

[b] Mg# = Molar Mg/(Mg + Fe^{2+}) assuming an Fe^{2+}/Fe_{Tot} ratio of 0.85.

[c] calculated based on degree of crystallinity assuming component increases incompatibly (value not included in total).

Mineral abbreviations are as in Table 2.3.

Table 2.4. Computed compositions of bulk solids of the mineral assemblages from computed phase abundances of Table 2.3 for IRVsynth (0.01 wt.% bulk water[a]) at 2.8 kbars.

Experiment (No.)	IRV018dr	IRV019dr	IRV020dr
Temperature (°C)	1150	1125	1100
SiO_2	35.69	31.00	30.07
TiO_2	0.06	0.07	0.05
Al_2O_3	0.12	0.04	0.05
Cr_2O_3	0.35	0.20	0.15
FeO	32.85	40.43	41.56
MnO	0.58	0.56	0.47
MgO	29.84	26.46	27.17
CaO	0.31	0.35	0.34
Na_2O	0.08	0.01	0.00
K_2O	0.02	0.00	0.01
P_2O_5	0.10	0.87	0.13
Total	100.00	100.00	100.00
Mg#[b]	66	58	58

~ from phase abundances

[a] measured by FTIR.

[b] Mg# = Molar Mg/(Mg + Fe^{2+}) assuming an Fe^{2+}/Fe_{Tot} ratio of 0.85.

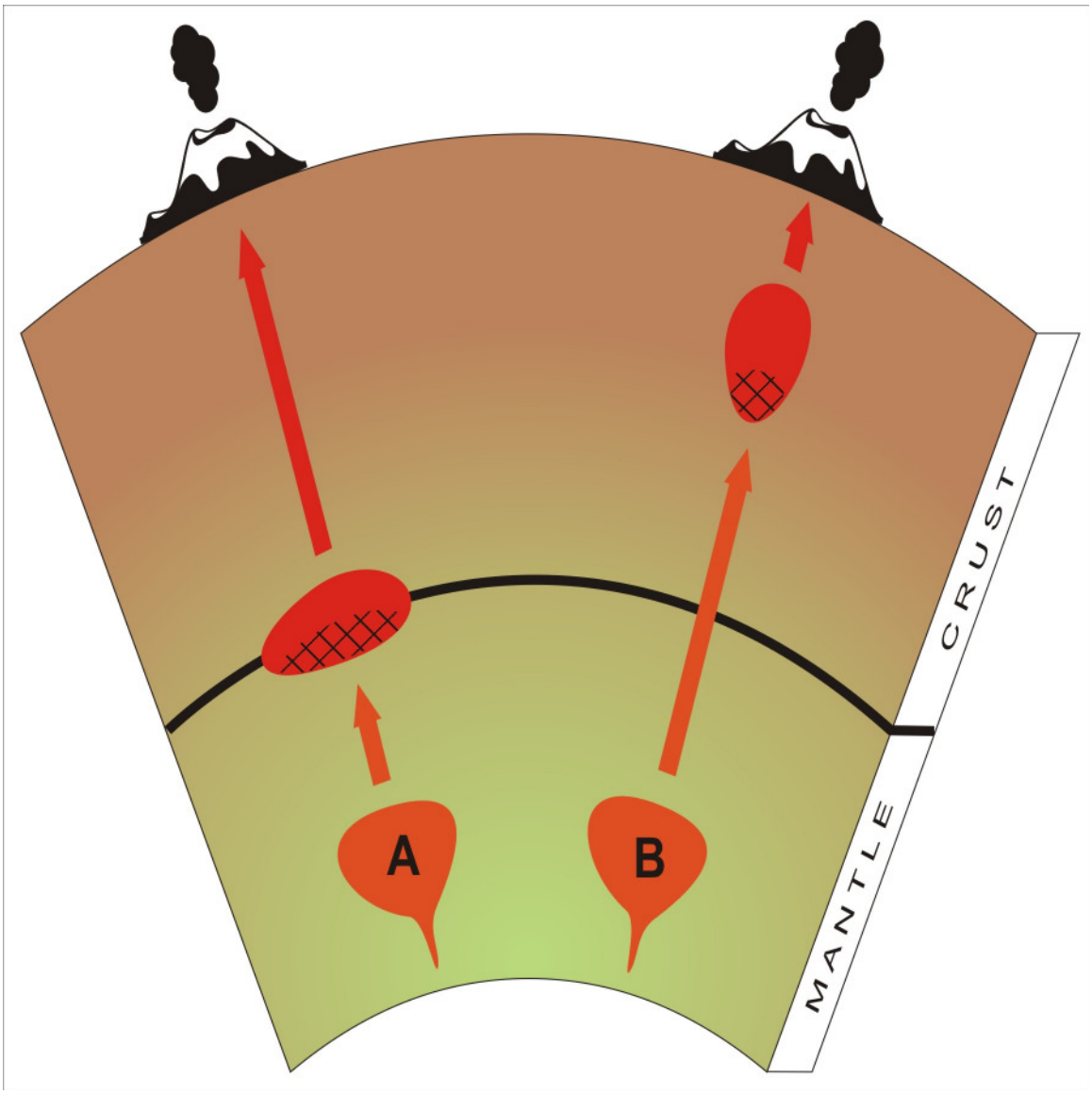

Figure 2.1. Schematic illustrating the process of single-stage fractional crystallization at two depths; one at the base of a thick crust in which liquids residual to fractionation ascend to the surface or subsurface (A) and the second at mid-crustal region (B).

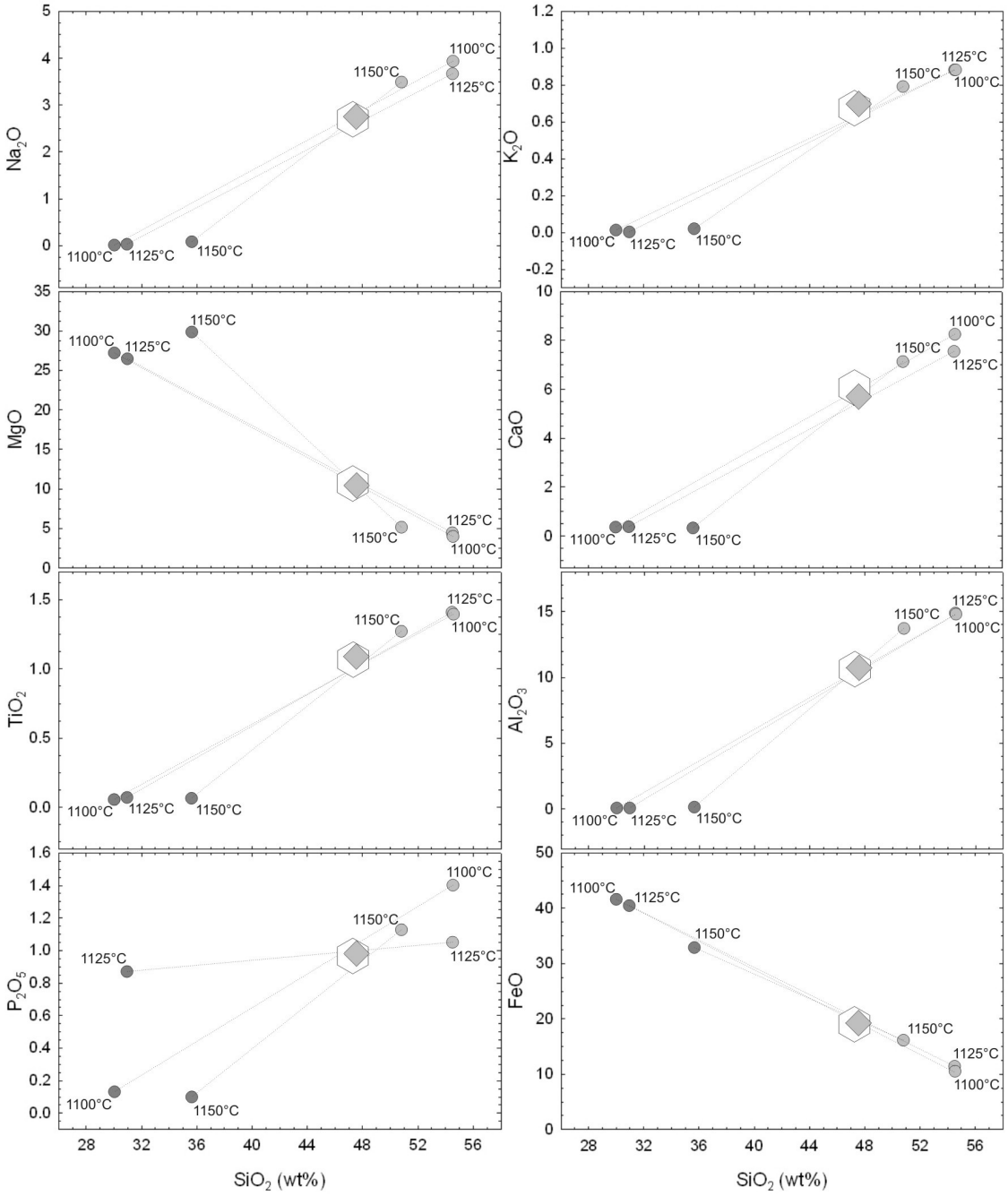

Figure 2.2. Harker-variation diagram for residual liquids (grey circles) and bulk solids (dark grey circles) from experiments on Irvine with 0.01 wt.% H_2O at 2.8 kbars. Irvine bulk rock composition analyzed by rover Spirit re-normalized after subtracting out volatiles (SO_3) (open hexagon) and IRVsynth (grey diamonds) are also represented. Tielines connect residual liquid and solid phases co-existing at the indicated temperature.

Bibliography

Abbott M.J. (1969) Petrology of the Nandewar Volcano, N.S.W., Australia. *Contributions to Mineralogy and Petrology* **20**, 115-134.

Anderson D.J., Lindsley D.H. and Davidson P.M. (1993) QUILF- a Pascal program to assess equilibria among Fe-Mg-Mn-Ti oxides, pyroxenes, olivine, and quartz. *Computers and Geosciences* **19**, 1333-1350.

Bandfield J.L., Hamilton V.E., Christensen P.R. and McSween H.Y. (2004) Identification of quartzofeldspathic materials on Mars. *Journal of Geophysical Research-Planets* **109**, E10009.

Bertka C.M. and Fei Y. (1998) Density profile of an SNC model Martian interior and the moment-of-inertia factor for Mars. *Earth and Planetary Science Letters* **157**, 79-88.

Bishop J.L., Noe Dobrea E.Z., McKeown N.K., Parente M., Ehlmann B.L., Michalski J.R., Milliken R.E., Poulet F., Swayze G.A, Mustard J.F., Murchie S.L. and Bibring J.P. (2008) Phyllosilicate Diversity and Past Aqueous Activity Revealed at Mawrth Vallis, Mars. *Science* **321**, 10.1126/science.1159699.

Breuer D. and Spohn T. (2003) Early plate tectonics versus single-plate tectonics on Mars: Evidence from magnetic field history and crust evolution. *Journal of Geophysical Research-Planets* **108**(E7), 5072.

Carmichael I.S.E. (1964) The Petrology of Thingmuli, A tertiary volcano in eastern Iceland. *Journal of Petrology* **5**, 435-460.

Carmichael I.S.E., Turner F.J. and Verhoogen J. (1974) *Igneous Petrology.* 1st ed., 32 pp. McGraw-Hill Book Company

Carr M. J. (2002) IgPet for Windows, edited, Terra Softa Inc., Somerset, NJ.

Christensen P.R., Wyatt M.B., Glotch T.D., Rogers A.D., Anwar S., Arvidson R.E., Bandfield J.L., Blaney D.L., Budney C., Calvin W.M., Faracaro A., Fergason R.L., Gorelick N., Graff T.G., Hamilton V.E., Hayes A.G., Johnson J.R., Knudson A.T., McSween H.Y., Mehall G.L., Mehall L.K., Moersch J.E., Morris R.V., Smith M.D., Squyres S.W., Ruff S.W. and Wolff M.J. (2004) Mineralogy at Meridiani Planum from Mini-TES Experiment on the Opportunity Rover. *Science* **306,** 5702-1733.

Christensen P.R., McSween H.Y., Bandfield J.L., Ruff S.W., Rogers A.D., Hamilton V.E., Gorelick N., Wyatt M.B., Jakosky B.M., Kieffer H.H., Malin M.C. and Moersch J.E. (2005) Evidence for magmatic evolution and diversity on Mars from infrared observations. *Nature* **436**, 882-882.

DiFrancesco N.J., Whitaker M.L., Nekvasil H. and Lindsley D.H. (2003) A road to rhyolite: fractional crystallization experiments on a continental olivine tholeiite. *Geological Society of America* **35**, 631.

Dreibus G. and Wänke H. (1985) Mars: a volatile-rich planet. *Meteoritics* **20**, 367-382.

Elardo S.M., Harrington A.D., Nekvasil H., McCubbin F.M. and Lindsley D.H. (2008) Constraints on water contents of martian magmas: Inferences from the Chassigny meteorite and experiments on Backstay. *Lunar and Planetary Science XXXIX*. Lunar Planet. Inst., Houston. #1802 (abstr.).

Eugster H.P. and Skippen G.B. (1967) Igneous and metamorphic reactions involving gas equilibria. *Researches in Geochemistry*, edited by P.H. Abelson, pp. 492-520, John Wiley, New York.

Filiberto J. and Nekvasil H. (2003) Linking tholeiites and silica-undersaturated alkalic rocks: an experimental study. *GSA Abstracts with Programs **34***, 258-216.

Frey F.A., Garcia M.O., Wise W.S., Kennedy A., Gurriet P. and Albarede F. (1991) The evolution of Mauna-Kea volcano, Hawaii - petrogenesis of tholeiitic and alkalic basalts. *Journal of Geophysical Research-Solid Earth and Planets* **96**, 14347-14375.

Frost B.R., Frost C.D., Lindsley D.H., Scoates J.S. and Mitchell J.N. (1993) The Laramie Anorthosite Complex and Sherman Batholith: geology, evolution, and theories of origin. In: Snoke, A. W., Steidtmann, J. R. & Roberts, S. (eds) *Geology of Wyoming. Geological Survey of Wyoming Memoir* **5**, 118-161.

Frost C.D. and Frost B.R. (1997) Reduced rapakivi-type granites: The tholeiite connection. *Geology* **25**, 647-650.

Geist D., Howard K.A. and Larson P. (1995) The generation of oceanic rhyolites by crystal fractionation - The basalt-rhyolite association at volcan-alcedo, Galapagos-Archipelago. *Journal of Petrology* **36**, 965-982.

Gellert R., Rieder R., Brückner J., Clark B.C., Dreibus G., Klingelhöfer G., Lugmair G., Ming D.W., Wänke H., Yen A., Zipfel J. and Squyres S.W. (2006). Alpha Particle X-Ray Spectrometer (APXS): Results from Gusev crater and calibration report. *Journal of Geophysical Research-Planets* **111**, E02S05.

Hahn B.C. and McLennan S.M. (2007) The bulk chemical composition of the upper martian crust. *Geochimica Et Cosmochimica Acta* **71**, A369-A369.

Hurowitz J.A., McLennan S.M., McSween H.Y., de Souza, Jr., P.A. and Klingelhöfer G. (2006) Mixing relationships and the effects of secondary alteration in the Wishstone and Watchtower Classes of Husband Hill, Gusev Crater, Mars. *Journal of Geophysical Research-Planets* **111**, E12S14.

Irvine T.N. and Baragar W.R.A. (1971). Guide to chemical classification of common volcanic rocks. *Canadian Journal of Earth Sciences* **8**, 523-548.

Karner J.M., Papike J.J., Shearer C.K., McKay G., Le L. and Burger P. (2007) Valence state partitioning of Cr and V between pyroxene-melt: Estimates of oxygen fugacity for martian basalt QUE 94201. *American Mineralogist*, **92**, 1238-1241.

MacDonald G.A. and Katsura T. (1964) Chemical Composition of Hawaiian Lavas. *Journal of Petrology* **5**, 83-133.

Mandeville C.W., Webster J.D., Rutherford M.J., Taylor B.E., Timbal A. and Faure K. (2002) Determination of molar absorptivities for infrared absorption bands of H2O in andesitic glasses. *American Mineralogist* **87**, 813-821.

McCubbin F.M. and Nekvasil H. (2008) Maskelynite-hosted apatite in the Chassigny meteorite: Insights into late-stage magmatic volatile evolution in martian magmas. *American Mineralogist* **93**, 676-684.

McCubbin F.M., Nekvasil H., Harrington A.D., Elardo S.M. and Lindsley D.H. (2008) Compositional diversity and stratification of the martian crust: Inferences from crystallization experiments on the picrobasalt Humphrey from Gusev Crater, Mars. *Journal of Geophysical Research-Planets* **113**, E11013.

McCubbin F.M., Smirnov A., Nekvasil H., Lindsley D.H., Wang J., and Hauri E.H. (In prep) Hydrous magmatism on Mars: A source for water on the ancient martian surface and the current martian subsurface? *Science*.

McSween H.Y., Grove T.L. and Wyatt M.B. (2003) Constraints on the composition and petrogenesis of the Martian crust. *Journal of Geophysical Research-Planets* **108**(E12), 5135.

McSween H.Y., Ruff S.W., Morris R.V., Bell J.F., Herkenhoff K., Gellert R., Stockstill K.R., Tornabene L.L., Squyres S.W., Crisp J.A., Christensen P.R., McCoy T.J., Mittlefehldt D.W. and Schmidt M. (2006a) Alkaline volcanic rocks from the Columbia Hills, Gusev Crater, Mars. *Journal of Geophysical Research-Planets* **111**, E09S91.

McSween H.Y., Wyatt M.B., Gellert R., Bell III, J.F., Morris R.V., Herkenhoff K.E., Crumpler L.S., Milam K.A., Stockstill K.R., Tornabene L.L., Arvidson R.E., Bartlett P., Blaney D., Cabrol N.A., Christensen P.R., Clark B.C., Crisp J.A., Des Marais D.J., Economou T., Farmer J.D., Farrand W., Ghosh A., Golombek M., Gorevan S., Greeley R, Hamilton V.E., Johnson J.R., Joliff B.L., Klingelhöfer G., Knudson A.T., McLennan S., Ming D., Moersch J.E., Rieder R., Ruff S.W., Schröder C., de Souza, Jr., P.A., Squyres S.W., Wänke H., Wang A., Yen A. and Zipfel J. (2006b) Characterization and petrologic interpretation of olivine-rich basalts at Gusev Crater, Mars, *Journal of Geophysical Research-Planets* **111**, E02S10.

Ming D.W., Mittlefehldt D.W., Morris R.V., Golden D.C., Gellert R., Yen A., Clark B.C., Squyres S.W., Farrand W.H, Ruff S.W., Arvidson, Klingelhöfer G., McSween H.Y., Rodionov D.S., Schröder C., de Souza, Jr., P.A. and Wang A. (2006) Geochemical and mineralogical indicators for aqueous processes in the Columbia Hills of Gusev crater, Mars. *Journal of Geophysical Research-Planets* **111,** E02S12.

Monders A.G., Médard E. and Grove T.L. (2007) Phase equilibrium investigations of the Adirondack class basalts from the Gusev plains, Gusev crater, Mars. *Meteoritics and Planetray Science*. **42**, 131-148.

Morgan G.B. and London D. (1996) Optimizing the electron microprobe analysis of hydrous alkali aluminosilicate glasses. *American Mineralogist*. **81**, 1176–1185.

Morgan G.B. and London D. (2005) Effect of current density on the electron microprobe analysis of alkali aluminosilicate glasses. *American Mineralogist*. **90**, 1131–1138.

Nekvasil H., Simon A. and Lindsley D.H. (2000) Crystal fractionation and the evolution of intra-plate hy-normative igneous suites: insights from their feldspars. *Journal of Petrology* **41**(12), 1743–1757.

Nekvasil H., Lindsley D.H., Whitaker M.L., Filiberto J., DiFrancesco N.J., Rossier L. and Horn J. (2003) Tholeiites, anorthosites, potassic granites, sodic trachytes, and tephriphonolites: is there a link? *Geological Society of America. Abstracts with Programs* **35**, 395.

Nekvasil H, Filiberto J., Whitaker M. and Lindsley D.H. (2003), Magmas parental to the Chassigny meteorite: New considerations. 6th International Conference on Mars, Pasadena, CA. Abstract No. 3041.

Nekvasil H., Dondolini A., Horn J., Filiberto J., Long H. and Lindsley D. H. (2004) The origin and evolution of silica-saturated alkalic suites: an experimental study. *Journal of Petrology.* **45***,* 693–721.

Nekvasil H, Filiberto J., McCubbin F.M., Lindsley D.H. (2007a) Alkalic parental magmas for the chassignites? *Meteoritics and Planetary Science* ***42***, 979-992.

Nekvasil H., McCubbin F.M., Harrington A.H., O'Leary M.C., Elardo S.M. and Lindsley D.H. (2007b) Crustal differentiation on Mars: Insights from rocks analyzed by the MER rovers. 7th International Conference on Mars, Pasadena, CA. Abstract No. 3181.

Nekvasil H., McCubbin F.M., Harrington A.D., Elardo S.M. and Lindsley, D.H. (submitted) Linking the Chassigny meteorite and the martian surface rock Backstay: Insights into igneous crustal differentiation processes on Mars. *Meteoritics and Planetary Science.*

Norman M. D. (1999) The composition and thickness of the crust of Mars estimated from rare earth elements and neodymium-isotopic compositions of martian meteorites, *Meteoritics and Planetary Science* **34**, 439-449.

Norman M.D. (2002) Thickness and Composition of the Martian Crust Revisited: Implications of an Unltradepleted Mantle with a Nd Isotopic Composition like that of QUE94201. *Lunar and Planetary Science XXXIII*. Lunar Planet. Inst., Houston. #1175 (abstr.).

Rogers A.D. and Aharonson O. (2008) Mineralogical composition of sands in Meridiani Planum determined from Mars Exploration Rover data and comparison to orbital measurements. *Journal of Geophysical Research-Planets* **113**, E06S14.

Scoates J.S., Frost C.D., Mitchell J.N., Lindsley D.H. and Frost B.R. (1996) Residual-liquid origin for a monzonitic intrusion in a mid-Proterozoic anorthosite complex: The Sybille intrusion, Laramie anorthosite complex, Wyoming. *Geological Society of America Bulletin* **108**, 1357-1371.

Spulber S.D. and Rutherford M.J. (1983) The Origin of Rhyolite and Plagiogranite in Oceanic Crust: And Experimental Study. *Journal of Petrology* **24**(1), 1-25.

Stolz A. J. (1985) The role of fractional crystallization in the evolution of the Nandewar Volcano, northeastern New South Wales, Australia. *Journal of Petrology* **26**, 1002–1026.

Squyres S.W., Arvidson R.E., Blaney D.L., Clark B.C., Crumpler L., Farrand W.H., Gorevan S., Herkenhoff K.E., Hurowitz J., Kusack A., McSween H.Y., Ming D.W., Morris R.V., Ruff S.W., Wang A. and Yen A. (2006) Rocks of the Columbia Hills. *Journal of Geophysical Research-Planets* **111**, E02S11

Taylor G.J., Boynton W., Brueckner J., Wänke H., Dreibus G., Kerry K., Keller J., Reedy R., Evans L., Starr R., Squyres S., Karunatillake S., Gasnault O., Maurice S., d'Uston C., Englert P., Dohm J., Baker V., Hamara D., Janes D., Sprague A., Kim K., Drake D. (2006) Bulk composition and early differentiation of Mars. *Journal of Geophysical Research-Planets* **111**, E03S10.

Taylor S.R. (1989) Growth of Planetary Crusts. *Tectonophysics* **161**, 147-156.

Taylor S.R. (2001) *Solar System Evolution: A new Perspective.*, 2nd ed., 460 pp., Cambridge University Press.

Taylor S.R. and McLennan S.M. (2009) *Planetary Crusts: Their Composition, Origin and Evolution.*, 1st ed., 164 pp., Cambridge Planetary Science.

Whitaker M.L., Nekvasil H., Lindsley D.H. and Difrancesco N.J. (2007a) The role of pressure in producing compositional diversity in intraplate basaltic magmas. *Journal of Petrology* **48**, 365-393.

Whitaker M.L., Lindsley D.H., Whitaker J.M.K. and Nekvasil H. (2007b). Carbon is not required during crystallization to produce ferrobasalts/ferrodiorites (FTP rocks). *American Mineralogist* **92**, 1750-1755.

Whitaker M.L., Nekvasil H., Lindsley D.H. and McCurry M. (2008) Can crystallization of olivine tholeiite give rise to potassic rhyolites? an experimental investigation. *Bulletin of Volcanology* **70**, 417-434.

Wieczorek M.A. and Zuber M.T. (2004) Thickness of the martian crust: Improved constraints from geoid-to-topography ratios, *Journal of Geophysical Research.-Planet* **109**, E01009.

Winter J.D. (2001) *An Introduction to Igneous and Metamorphic Petrology*. 1st ed., 250 pp., Prentice Hall Press.

Yoder H.S. and Tilley C.E. (1962) Origin of basalt magmas: an experimental study of natural and synthetic rock systems. *Journal of Petrology* **3**, 342-532.

Zimbelman J.R., Solomon S.C. and Sharpton V.L. (1991) The Evolution of Volcanism, Tectonics, and Volatiles on Mars: An Overview of Recent Progress. *Proceedings of Lunar and Planetary Science* **21**, 613-626.